AERIAL MANIPULATION FOR INDOOR APPLICATIONS

BY

ROBERT MITCHELL JONES

THESIS

Submitted in partial fulfillment of the requirements
for the degree of Master of Science in Mechanical Engineering
in the Graduate College of the
University of Illinois at Urbana-Champaign, 2017

Urbana, Illinois

Adviser:

Professor Naira Hovakimyan

ABSTRACT

This thesis presents the design and control of a small aerial manipulator operating in indoor environments. The critical challenges of functioning effectively in such environments are (i) maximizing workspace in constrained spaces like narrow corridors or tight corners, and (ii) achieving stable flight when carrying payloads of unknown mass in the presence of uncertainties. While aerial manipulation has been researched to some extent, few efforts have been made to address both of these challenges simultaneously.

First, the dynamics of the quadrotor and manipulator are introduced. Then, two types of baseline flight controllers are described as well as a feedforward torque compensation controller and a robust adaptive augmenting controller. Next, the vehicle and manipulator design methodology is discussed. Lastly, results from the implementation of these algorithms on a real aerial manipulator are presented and conclusions of their efficacy are drawn.

ACKNOWLEDGMENTS

I would first like to thank my adviser Prof. Naira Hovakimyan for her continuing support and advice throughout my time here at The University of Illinois at Urbana-Champaign.

I thank my fellow labmates at the Advanced Controls Research Lab: Arun Lakshmanan, Thiago Marinho, Gabriel Barsi Haberfeld, Andrew Patterson, and everyone else at ACRL for their stimulating discussions, for the sleepless nights in IRL preparing for deadlines and demos, and for all the fun we had over the past two years.

Last but not least, I would like to thank my parents and siblings for their love and support throughout my life and academic career.

TABLE OF CONTENTS

CHAPTER 1

INTRODUCTION

Manipulators have played, and continue to play, a very important role in today's technological society. Most large manufacturing facilities use manipulators for tasks ranging from the assembly of computer chips to the construction of electric cars. These machines are extremely good at their job due to their superior speed and precision as compared with humans, however, this comes at a cost. In order to achieve this level of performance, these robotic arms must have very stiff components and very powerful motors. Consequently, they are usually very large and heavy. For most manufacturing applications this is not a problem since the manipulators are mounted to a concrete floor in their designated workspace. However, in non-industrial applications sub-millimeter precision may not be required, thus eliminating the need for such large stationary machines.

In many cases, it may be necessary to have a manipulator with a moving base. The task of fetching and carrying objects in the home or office is a good example where a mobile manipulator could perform well and be extremely useful. Researchers from the University of Illinois recieved funding from NSF to work on a project "Automation Supporting Prolonged Independent Residence for the Elderly" (ASPIRE) to explore the use of small aerial and ground co-robots in domestic environment [1]. Study shows that for the types of daily activity assistance, fetching objects from the floor or another room, reaching for objects, and finding/delivering items are among those tasks which are preferred to be completed by robot [2]. Under this research framework, an aerial vehicle appropriate for indoor use was designed and augmented with a manipulator so that it can pick up common household items for people with reduced mobility such as medicine bottles, reading glasses, and cell phones, etc. in Figure 1.1. Small aerial vehicles are agile and have the advantage in completing this sort of task over ground vehicles, which are not capable of climbing stairs or reaching for items far from the

ground.

Aerial manipulators have recently gained interest in the controls and robotics community as multirotors have become more accessible. Reference [3] presented the design of several light-weight, low-complexity grippers that allow quadrotors to grasp and perch on branches or beams and pick up and transport payloads. While their method allows for grasping a wide range of objects and materials, their vehicle is required to fly directly over the top of the payload and often punctures the object with the gripper hooks. An algorithm for aerial grasping of moving targets was presented in [4], where two classes of canonical grasping maneuvers were defined and characterized, and a planning strategy relying on differential flatness was then proposed to concatenate on one or more grasping maneuvers. However, the single link design of this aerial manipulator does not allow for the payload to be moved close to the center of mass of the vehicle, preventing passage through small spaces. Reference [5] introduced a quadrotor manipulation system using a 2-link manipulator, proposing a solution to the drawbacks found in the design with grippers fixed to a quadrotor. The proposed system enables the end-effector to achieve arbitrary orientation. A controller based on feedback linearization was designed to track desired trajectories. In [6, 7] a design was proposed that equipped a quadrotor MAV with an actuated appendage to enable grasping and retrieval of objects at high speeds, and differential flatness property was used to plan dynamic trajectories. A Lyapunov based model reference adaptive control design for aerial manipulation was presented in [8] for an aerial vehicle with dual multi degrees of freedom manipulators. A control system based on feedback linearization and PD control was proposed in [9] for an aerial manipulator taking into account the mutual reactive influence of the robotic manipulator and the UAV. In [10], a six degree of freedom parallel manipulator was designed to robustly maintain precise end-effector positioning in the presence of perturbations, and was compared with a serial manipulator. For unknown payload, [11] proposed an on-line estimator based on parametrization of the aerial manipulator dynamics to evaluate the unknown payload, and a passivity-based control algorithm was designed to control the system. Study in [12] developed and validated a nonlinear model-predictive control methodology to achieve optimized performance in pick-and-place tasks of aerial manipulators. The approach employed a sequential Newton method

for unconstrained optimal control and a high-frequency low-level controller to track the generated optimal reference trajectories. On-board vision system was used for object tracking.

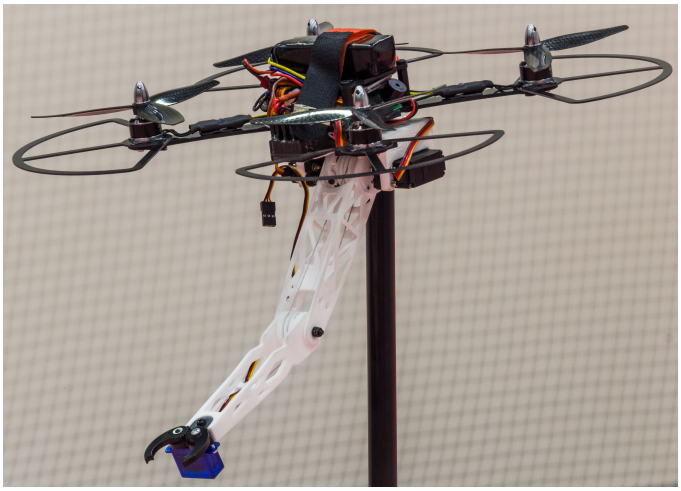

Figure 1.1: Autonomous Quadrotor with 2 DOF Manipulator Arm

This thesis discusses the design and control of a powerful aerial manipulator with suitable characteristics for indoor use. A mathematical framework for studying the dynamics of the aerial manipulator system will be introduced in Chapter 2. Control laws will be proposed in Chapter 3 to stabilize the coupled system. The physical design of the quadrotor and manipulator will be discussed in detail in Chapter 4. Lastly, Chapter 5 shows results from high-fidelity simulations and flight tests, verifying the efficacy of the proposed vehicle design and control scheme.

The addition of the manipulator to the quadrotor will introduce dynamically changing inertial properties, as well as internal torques and forces between the two subsystems. In addition, unknown payloads add to the uncertainty in system dynamics. To this end, a feedforward torque compensation controller is designed to reject the torque induced on the airframe by the manipulator itself. In addition, an $\mathcal{L}_1$ adaptive augmenting controller is shown to reject uncertainty introduced by unknown payloads and unmodeled dynamic effects. Before the control design could proceed, system identification and modeling was carried out to obtain basic model dynamics. Then control design for stabilization and manipulation were developed and tested in simulation and flight testing.

As much of this content has been published during the process of writing this thesis, the author would like to cite [13], and especially acknowledge the other authors for their contributions to this work.

CHAPTER 2

DYNAMIC MODEL

2.1 Vehicle Dynamics

2.1.1 Coordinate System

We start the discussion of dynamics by first introducing the coordinate frames as well as the mapping between them. Since this vehicle's primary place of operation is inside homes and buildings, a right-handed, z-up coordinate frame is chosen. We define x_W, y_W, z_W to be the axes in the inertial world frame $\mathcal{W}$ and x_B, y_B, z_B to be the axes in the vehicle body frame $\mathcal{B}$. We then define a rotation matrix to map coordinates between body frame and world frame

$$
\begin{aligned}
R_B^W &= R_{z,\psi} R_{y,\theta} R_{x,\psi} \\
&= \begin{bmatrix} c_\psi & s_\psi & 0 \\ -s_\psi & c_\psi & 0 \\ 0 & 0 & 1 \end{bmatrix} \begin{bmatrix} c_\theta & 0 & -s_\theta \\ 0 & 1 & 0 \\ s_\theta & 0 & c_\theta \end{bmatrix} \begin{bmatrix} 1 & 0 & 0 \\ 0 & c_\phi & s_\phi \\ 0 & -s_\phi & c_\phi \end{bmatrix} \\
&= \begin{bmatrix} c_\psi c_\theta & c_\psi s_\theta s_\phi - c_\phi s_\psi & s_\psi s_\phi + c_\psi c_\phi s_\theta \\ c_\theta s_\psi & c_\psi c_\phi + s_\psi s_\theta s_\phi & c_\phi s_\psi s_\theta - c_\psi s_\phi \\ -s_\theta & c_\theta s_\phi & c_\theta c_\phi \end{bmatrix}
\end{aligned}
$$

where c_α and s_α are abbreviations of $\cos(\alpha)$ and $\sin(\alpha)$ respectively.

Thus, using this rotation matrix, the axes in $\mathcal{B}$ can be mapped to $\mathcal{W}$ as

$$\begin{aligned} x_B &= R_B^W \begin{bmatrix} 1 & 0 & 0 \end{bmatrix}^\top \\ y_B &= R_B^W \begin{bmatrix} 0 & 1 & 0 \end{bmatrix}^\top \\ z_B &= R_B^W \begin{bmatrix} 0 & 0 & 1 \end{bmatrix}^\top . \end{aligned}$$

2.1.2 Translational Equations of Motion

We define the translational acceleration of the vehicle in $\mathcal{W}$ by summing the total thrust force exerted by the quadrotor with the force due to gravity:

$$\begin{aligned} m\ddot{x} &= -mgz_W + u_f z_B \\ \ddot{x} &= -gz_W + \frac{u_f}{m} z_B, \end{aligned}$$

where $x \in \mathbb{R}^3$ is the position vector of the vehicle in $\mathcal{W}$, m is the mass of the vehicle, g is the gravitational constant, and $u_f \in \mathbb{R}$ is the sum of the thrust exerted by all of the motors.

2.1.3 Rotational Equations of Motion

Assume a diagonal inertia tensor $\mathcal{I}$ written as

$$\mathcal{I} = \begin{bmatrix} \mathcal{I}_{xx} & 0 & 0 \\ 0 & \mathcal{I}_{yy} & 0 \\ 0 & 0 & \mathcal{I}_{zz} \end{bmatrix},$$

where $\mathcal{I}_{xx}, \mathcal{I}_{yy}, \mathcal{I}_{zz} \in \mathbb{R}$ are the vehicle's moment of inertia about its x, y, z axes in $\mathcal{B}$ respectively.

We wish to find an expression for the angular acceleration dynamics of the quadrotor as a function of vehicle properties and the total moments acting on the body. The total moment acting on the vehicle can be written as

$$u_c = \begin{bmatrix} u_{c1} \\ u_{c2} \\ u_{c3} \end{bmatrix} = u_m + u_a = \begin{bmatrix} u_\phi \\ u_\theta \\ u_\psi \end{bmatrix} + \begin{bmatrix} 0 \\ \tau_m \\ 0 \end{bmatrix}$$

where $[u_\phi, u_\theta, u_\psi]^\top \in \mathbb{R}^3$ are the moments from the propellers in the roll, pitch, and yaw directions respectively, and τ_m is the torque induced by the manipulator in the pitch direction, to be defined in the following section.

We can write the the relationship between input torque and rotational states as

$$\begin{aligned} u_c &= \frac{d}{dt} H \\ u_c &= \frac{\partial}{\partial t} H + \Omega_B \times H \\ u_c &= \mathcal{I} \cdot \dot{\Omega}_B + \Omega_B \times (\mathcal{I} \cdot \Omega_B), \end{aligned}$$

where H is the angular momentum of the quadrotor in $\mathcal{B}$, and $\Omega_B = [p, q, r]^\top \in \mathbb{R}^3$ is the angular velocity of the vehicle in $\mathcal{B}$ in the roll, pitch, and yaw direction respectively. The angular accelerations in $\mathcal{B}$ are

$$\dot{\Omega}_B = \mathcal{I}^{-1} \left(-\Omega_B \times \mathcal{I} \cdot \Omega_B + u_c \right)$$

$$\begin{bmatrix} \dot{p} \\ \dot{q} \\ \dot{r} \end{bmatrix} = \begin{bmatrix} \frac{1}{\mathcal{I}_{xx}} & 0 & 0 \\ 0 & \frac{1}{\mathcal{I}_{yy}} & 0 \\ 0 & 0 & \frac{1}{\mathcal{I}_{zz}} \end{bmatrix} \left(\begin{bmatrix} (\mathcal{I}_{yy} - \mathcal{I}_{zz})\, qr + u_{c1} \\ (\mathcal{I}_{zz} - \mathcal{I}_{xx})\, pr + u_{c2} \\ (\mathcal{I}_{xx} - \mathcal{I}_{yy})\, pq + u_{c3} \end{bmatrix} \right).$$

The angular acceleration about each axis in $\mathcal{B}$ can then be written as

$$\begin{aligned} \dot{p} &= \frac{1}{\mathcal{I}_{xx}} \left((\mathcal{I}_{yy} - \mathcal{I}_{zz})\, qr + u_{c1} \right) \\ \dot{q} &= \frac{1}{\mathcal{I}_{yy}} \left((\mathcal{I}_{zz} - \mathcal{I}_{xx})\, pr + u_{c2} \right) \\ \dot{r} &= \frac{1}{\mathcal{I}_{zz}} \left((\mathcal{I}_{xx} - \mathcal{I}_{yy})\, pq + u_{c3} \right). \end{aligned}$$

2.1.4 Motor Mapping

Once a desired control signal $u = [u_f, u_\phi, u_\theta, u_\psi]^\top$ is computed, it must be transformed to give individual actuator commands $[u_1, u_2, u_3, u_4]$. The map-

ping is as follows:

$$\begin{bmatrix} u_f \\ u_\phi \\ u_\theta \\ u_\psi \end{bmatrix} = \begin{bmatrix} k_F & k_F & k_F & k_F \\ -\frac{k_F}{\sqrt{2}}L & -\frac{k_F}{\sqrt{2}}L & \frac{k_F}{\sqrt{2}}L & \frac{k_F}{\sqrt{2}}L \\ -\frac{k_F}{\sqrt{2}}L & \frac{k_F}{\sqrt{2}}L & \frac{k_F}{\sqrt{2}}L & -\frac{k_F}{\sqrt{2}}L \\ -k_Q & k_Q & -k_Q & k_Q \end{bmatrix} \begin{bmatrix} u_1 \\ u_2 \\ u_3 \\ u_4 \end{bmatrix},$$

where k_F is the thrust coefficient, k_Q is the torque coefficient, and L is length of the quadrotor arm. Using a matrix inversion we can calculate the control signal in terms of individual motors as

$$\begin{bmatrix} u_1 \\ u_2 \\ u_3 \\ u_4 \end{bmatrix} = \frac{1}{4} \begin{bmatrix} \frac{1}{k_F} & -\frac{\sqrt{2}}{k_F L} & -\frac{\sqrt{2}}{k_F L} & -\frac{1}{k_Q} \\ \frac{1}{k_F} & -\frac{\sqrt{2}}{k_F L} & \frac{\sqrt{2}}{k_F L} & \frac{1}{k_Q} \\ \frac{1}{k_F} & \frac{\sqrt{2}}{k_F L} & \frac{\sqrt{2}}{k_F L} & -\frac{1}{k_Q} \\ \frac{1}{k_F} & \frac{\sqrt{2}}{k_F L} & -\frac{\sqrt{2}}{k_F L} & \frac{1}{k_Q} \end{bmatrix} \begin{bmatrix} u_f \\ u_\phi \\ u_\theta \\ u_\psi \end{bmatrix}.$$

2.2 Manipulator Dynamics

2.2.1 Servo Motor Dynamics

Standard servo motors possess several attributes which make them unique to many other types of electric motors. They can vary significantly in size, speed, and power but are usually comprised of the same basic components. A small DC electric motor, usually ranging from between 6 and 12 V, is used to produce torque and rotate the output shaft. A set of compound spur gears with a large gear reduction connects to the high speed DC motor and gives a low-speed, high-torque output. Physical stops on the output shaft limit the range of motion to between 90 and 180 degrees. For analog servo motors, a potentiometer measures the position of the output shaft. For digital servo motors, an absolute encoder is used to measure shaft position. A small integrated circuit reads measurements from the position sensor and controls the voltage to the DC motor in order to achieve a desired position.

To describe the dynamics of a DC servo motor we must first define the

saturation function:

$$a = sat(b, T) = \begin{cases} T, & \text{if } b > T \\ b, & \text{if } -T \leq b \leq T \\ -T, & \text{if } b < -T \end{cases},$$

where $T \in \mathbb{R}$ is the saturation limit and $a, b \in \mathbb{R}$.

We can now write the dynamics of the servo motor as

$$\ddot{\alpha} = sat\left(-k_{vis}\dot{\alpha} + sat\left(k_p\left(\alpha_d - \alpha\right), T_c\right), T_a\right),$$

where $\alpha \in \mathbb{R}$ is the angular state of the motor, $k_{vis}, k_p \in \mathbb{R}$ are the viscous friction constant and proportional control gain respectively, and T_c, T_a are the control saturation and torque saturation respectively.

2.2.2 2-Link Manipulator Dynamics

Planar serial manipulators have been widely studied in academia and complete descriptions of their kinematics and dynamics have become readily available. Based on the dynamics presented in [14], the planar rotational dynamics of this manipulator can be described as follows. Take the Lagrangian to be the total energy of the system.

Assume that the length of the first link is l_a and the first link is attached to the center of mass, A, of the quadrotor. Also assume that the centers of mass of the two links are on the center line and have a distance of l_1 and l_2 from A and B respectively. Let m_1 and m_2 denote the mass of the first link and the second link; let J_0, J_1, and J_2 denote the moment of inertia of the quadrotor with respect to the center of mass, that of the first link with respect to A, and that of the second link with respect to B. Let $\theta(t) \in \mathbb{R}$ denote the pitch angle of the quadrotor, $\alpha(t) \in \mathbb{R}$ and $\beta(t) \in \mathbb{R}$ denote the angles between the two links and the vertical line respectively. Let $\tau(t)$, $\tau_1(t)$, and $\tau_2(t)$ denote the torque exerted on the quadrotor from the rotors, at the first joint A, and the second joint B. For this system, let $q(t)$ denote the generalized coordinate as

$$q(t) = [\theta(t), \alpha(t), \beta(t)]^\top.$$

Payloads are modeled as a point mass located at the end on the second link. Define l_b as the length of the second link. Let m_p be the mass of the payload. To incorporate this payload into our dynamic model, for simplicity, we compute the change mass and inertia of the second link caused by the payload. This newly defined second link, with parameters J_{2c}, m_{2c}, and l_{2c}, can be represented as

$$\begin{aligned} J_{2c} &= J_2 + m_p l_b^2 \\ m_{2c} &= m_2 + m_p \\ l_{2c} &= \frac{m_2 l_2 + m_p l_b}{m_2 + m_p} \end{aligned}$$

The rotational equation of motion of the aerial manipulator in this plane, using Euler-Lagrange equation, is given by

$$M(q(t))\ddot{q}(t) + C(q(t), \dot{q}(t))\dot{q}(t) = F(t) - G(q(t)),$$

where

$$M(q(t)) = \begin{bmatrix} J_0 & 0 & 0 \\ 0 & m_1 l_1^2 + m_{2c} l_a^2 + J_1 & m_{2c} l_a l_{2c} \cos(\alpha(t) - \beta(t)) \\ 0 & m_{2c} l_a l_{2c} \cos(\alpha(t) - \beta(t)) & m_{2c} l_{2c}^2 + J_{2c} \end{bmatrix},$$

$$C(q(t), \dot{q}(t)) = \begin{bmatrix} 0 & 0 & 0 \\ 0 & 0 & m_{2c} l_a l_{2c} \dot{\beta}(t) \sin(\alpha(t) - \beta(t)) \\ 0 & -m_{2c} l_a l_{2c} \dot{\alpha}(t) \sin(\alpha(t) - \beta(t)) & 0 \end{bmatrix},$$

$$F(t) = \begin{bmatrix} \tau(t) + \tau_1(t) + \tau_2(t) \\ \tau_1(t) \\ \tau_2(t) \end{bmatrix},$$

and

$$G(q(t)) = \begin{bmatrix} 0 \\ (m_1 l_1 + m_{2c} l_a) g \sin \alpha(t) \\ m_{2c} l_{2c} g \sin \beta(t) \end{bmatrix}.$$

The two links are actuated by DC servo motors which take angle command $\alpha_c(t)$ and $\beta_c(t)$. The aforementioned servo motor model is used to obtain an estimate of the link angles and their derivatives. The torques $\tau_1(t)$ and $\tau_2(t)$ can be computed by the following equations

$$\begin{bmatrix}\tau_1(t)\\ \tau_2(t)\end{bmatrix} = \begin{bmatrix} m_1 l_1^2 + m_{2c} l_a^2 + J_1 & m_{2c} l_a l_{2c} \cos(\alpha(t) - \beta(t)) \\ m_{2c} l_a l_{2c} \cos(\alpha(t) - \beta(t)) & m_{2c} l_{2c}^2 + J_{2c} \end{bmatrix} \begin{bmatrix}\ddot{\alpha}(t)\\ \ddot{\beta}(t)\end{bmatrix} + \begin{bmatrix} 0 & m_{2c} l_a l_{2c} \dot{\beta}(t) \sin(\alpha(t) - \beta(t)) \\ -m_{2c} l_a l_{2c} \dot{\alpha}(t) \sin(\alpha(t) - \beta(t)) & 0 \end{bmatrix} \begin{bmatrix}\dot{\alpha}(t)\\ \dot{\beta}(t)\end{bmatrix} + \begin{bmatrix} (m_1 l_1 + m_{2c} l_a) g \sin \alpha(t) \\ m_{2c} l_{2c} g \sin \beta(t) \end{bmatrix}. \tag{2.1}$$

The total moment induced upon the airframe by the manipulator is then given by

$$\tau_m(t) = \tau_1(t) + \tau_2(t).$$

CHAPTER 3

CONTROL DESIGN

In this chapter, design of control laws will be discussed. To facilitate control law design and testing, a Simulink model has been built to model the dynamics of the quadrotor and the manipulator. All control design will be tested in this environment. A feedforward control law is designed to reduce the effect of motion of the manipulator on the quadrotor so that the performance of the attitude control augmentation system (CAS) will not degrade. In addition, when a payload of unknown mass is gripped by the end effector, the disturbance torque introduced by this payload cannot be compensated for by the feedforward controller. To deal with this uncertainty, an $\mathcal{L}_1$ adaptive control augmentation is designed and tested.

3.1 General Control Structure

Figure 3.1 illustrates the general flight control structure for the aerial manipulator system.

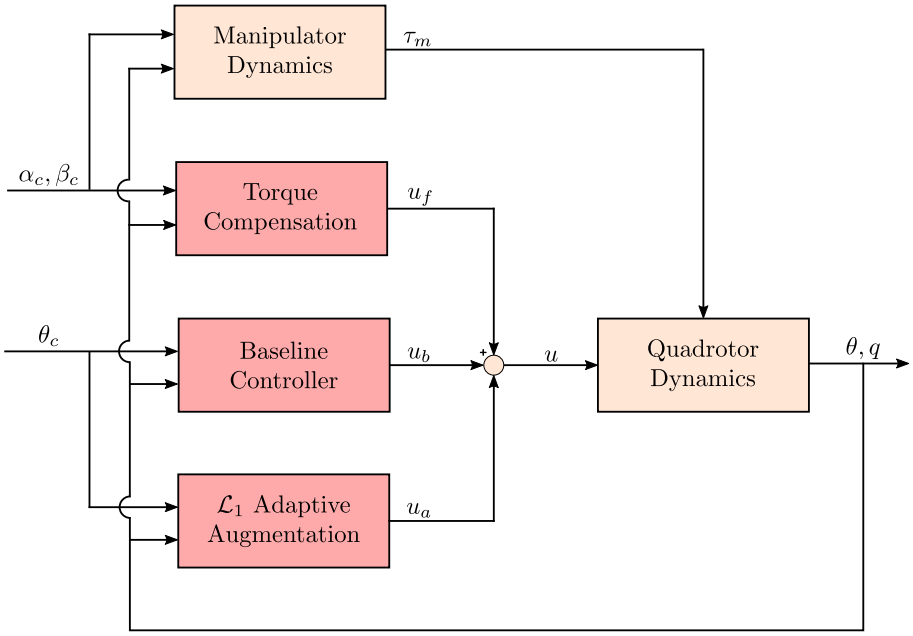

Figure 3.1: General control scheme

3.2 Baseline Flight Control

3.2.1 PI Control

The off-the-shelf baseline controller is an attitude tracking controller containing a PI rate CAS and a PID attitude CAS, see Figure 3.2. Let $\theta(t) \in \mathbb{R}$ denote the attitude angle of the vehicle, $\theta_c(t) \in \mathbb{R}$ denote the attitude angle command, $q(t) \in \mathbb{R}$ denote the associated rotational rate of the vehicle, and $q_c(t) \in \mathbb{R}$ denote the rotational rate command generated by the attitude CAS. Then the baseline control input $u_b(t)$ is given by

$$u_b(t) = k_{P1}\left(q_c(t) - q(t)\right) + k_{I1}\int_0^t \left(q_c(\tau) - q(\tau)\right) d\tau, \tag{3.1}$$

where

$$q_c(t) = k_{P2}\left(\theta_c(t) - \theta(t)\right) + k_{I2}\int_0^t \left(\theta_c(\tau) - \theta(\tau)\right) d\tau + k_D q(t),$$

and k_{P1}, k_{I1}, k_{P2}, k_{I2}, $k_D \in \mathbb{R}$ are control gains. Tracking performance of the baseline control is shown in Chapter 5.

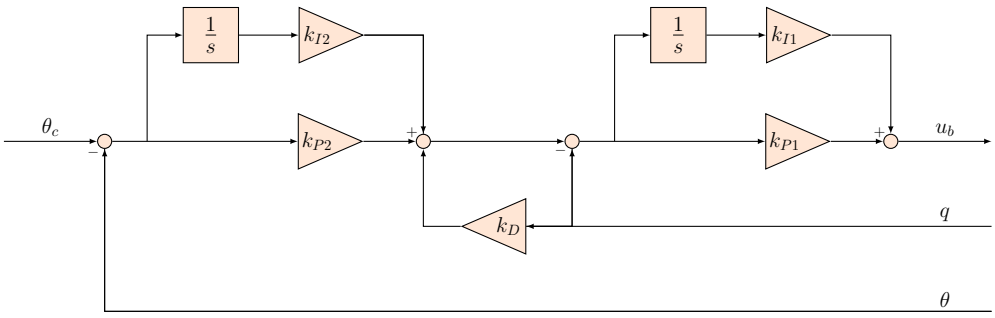

Figure 3.2: Baseline controller structure

3.2.2 Geometric Control

In many cases, like when executing highly dynamic maneuvers, the aforementioned PI baseline controller is not capable of tracking a given desired trajectory with satisfactory performance. To combat this trajectory tracking difficulty, a method proposed in [15] and expanded upon in [16] is employed. This geometric controller represents errors in the $SO\,(3)$ manifold in order to compute the desired rotational states.

From [16], a control signal is constructed as

$$u_b = \left[u_f, u_\phi, u_\theta, u_\psi\right]^\top$$

where $u_f \in \mathbb{R}^4$ is the desired thrust output and $u_\phi, u_\theta, u_\psi \in \mathbb{R}$ are the desired moments about each axis in the vehicle reference frame. The components of this control signal are computed as follows:

$$u_f = \left(K_x e_x + K_v e_v + mgz_W + m\ddot{x}_d\right) \cdot z_B,$$

where K_x, K_v are control gain matrices for position and velocity control re-

spectively, e_x, e_v are errors in position and velocity respectively, z_W is the z-axis of the inertial frame, z_B is body z-axis in inertial frame, $\ddot{x}_d \in \mathbb{R}^3$ is the desired acceleration, m is the vehicle mass, and g is the gravitational constant:

$$u_m = -K_R e_R - K_\Omega e_\Omega + \Omega_B \times \mathcal{I}\Omega_B - \mathcal{I}\left(\hat{\Omega}_B \left(R_B^D\right)^\top \Omega_D - \left(R_B^D\right)^\top \dot{\Omega}_D\right),$$

where $u_m = [u_\phi, u_\theta, u_\psi]^\top$, K_R, K_Ω are diagonal gain matrices for orientation and angular velocity respectively, e_R, e_Ω are errors in orientation and angular velocity respectively, $\Omega_B \in \mathbb{R}^3$ is the vehicle's angular velocity, $\Omega_D, \dot{\Omega}_D \in \mathbb{R}^3$ is the desired angular acceleration, and $\mathcal{I}$ is the vehicle's inertia matrix. The *hat* operator: $\hat{}$ is a mapping from $\mathbb{R}^3 \to SO(3)$.

3.3 Feedforward Torque Compensation

Since the model and parameters of the manipulator are well known, it is natural for the control signal to have a feedforward component, rejecting any torque that the manipulator induces on the airframe. A Lagrangian dynamic model of a serial manipulator is used to compute the manipulator torques. Since this model relies on knowledge of the angular states of the two links, a servo motor estimator is made to model the dynamics and internal controller of each servo motor.

Assuming the same geometric parameters as stated previously, the same rotational equation of motion of the aerial manipulator in the plane holds, and using Euler-Lagrange equation we have

$$M(q(t))\ddot{q}(t) + C(q(t), \dot{q}(t))\dot{q}(t) = F(t) - G(q(t)), \tag{3.2}$$

where,

$$M(q(t)) = \begin{bmatrix} J_0 & 0 & 0 \\ 0 & m_1 l_1^2 + m_{2c} l_a^2 + J_1 & m_{2c} l_a l_{2c} \cos(\alpha(t) - \beta(t)) \\ 0 & m_{2c} l_a l_{2c} \cos(\alpha(t) - \beta(t)) & m_{2c} l_{2c}^2 + J_{2c} \end{bmatrix},$$

$$C(q(t),\dot{q}(t)) = \begin{bmatrix} 0 & 0 & 0 \\ 0 & 0 & m_{2c}l_a l_{2c}\dot{\beta}(t)\sin(\alpha(t)-\beta(t)) \\ 0 & -m_{2c}l_a l_{2c}\dot{\alpha}(t)\sin(\alpha(t)-\beta(t)) & 0 \end{bmatrix},$$

$$F(t) = \begin{bmatrix} \tau(t)+\tau_1(t)+\tau_2(t) \\ \tau_1(t) \\ \tau_2(t) \end{bmatrix},$$

and

$$G(q(t)) = \begin{bmatrix} 0 \\ (m_1 l_1 + m_{2c} l_a) g \sin\alpha(t) \\ m_{2c} l_{2c} g \sin\beta(t) \end{bmatrix}.$$

Using the structure of the servo motor estimator described in 2, the angular states of each servo motor can be estimated. The torques $\hat{\tau}_1(t)$ and $\hat{\tau}_2(t)$ can be estimated by the following equations

$$\begin{aligned} \begin{bmatrix} \hat{\tau}_1(t) \\ \hat{\tau}_2(t) \end{bmatrix} &= \begin{bmatrix} m_1 l_1^2 + m_{2c} l_a^2 + J_1 & m_{2c} l_a l_{2c}\cos(\hat{\alpha}(t)-\hat{\beta}(t)) \\ m_{2c} l_a l_{2c}\cos(\hat{\alpha}(t)-\hat{\beta}(t)) & m_{2c} l_{2c}^2 + J_{2c} \end{bmatrix} \begin{bmatrix} \hat{\ddot{\alpha}}(t) \\ \hat{\ddot{\beta}}(t) \end{bmatrix} \\ &+ \begin{bmatrix} 0 & m_{2c} l_a l_{2c}\hat{\dot{\beta}}(t)\sin(\hat{\alpha}(t)-\hat{\beta}(t)) \\ -m_{2c} l_a l_{2c}\hat{\dot{\alpha}}(t)\sin(\hat{\alpha}(t)-\hat{\beta}(t)) & 0 \end{bmatrix} \begin{bmatrix} \hat{\dot{\alpha}}(t) \\ \hat{\dot{\beta}}(t) \end{bmatrix} \\ &+ \begin{bmatrix} (m_1 l_1 + m_{2c} l_a) g \sin\hat{\alpha}(t) \\ m_{2c} l_{2c} g \sin\hat{\beta}(t) \end{bmatrix}, \end{aligned} \tag{3.3}$$

where the $\hat{}$ denotes the estimated value. The feedforward command is then given by

$$u_f(t) = -(\hat{\tau}_1(t) + \hat{\tau}_2(t)).$$

3.4 $\mathcal{L}_1$ Adaptive Control Augmentation

The aerial manipulator can pick up a large variety of objects, varying in mass, inertia, density, shape, etc. With a flight controller augmented only with the feedforward torque compensation of the manipulator, there is no way to account for the induced torques and forces from these uncertain payloads. To reject uncertainties introduced by unknown payloads, the $\mathcal{L}_1$ adaptive control structure is chosen for its fast and robust adaptation.

An $\mathcal{L}_1$ adaptive control augmentation with piecewise constant adaptation law from [17] is proposed. Let $x_{I1}(t)$ and $x_{I2}(t)$ denote the states of the integrator

in the rate and attitude loops of the baseline controller respectively. Then, the rotational equation of motion of the quadrotor with the $\mathcal{L}_1$ augmentation can be expressed as

$$\begin{aligned}\dot{x}(t) &= A_m x(t) + B_r r(t) + B_m \left(u_a(t) + f_1(t,x)\right) + B_{um} f_2(t,x), \quad x(0) = x_0,\\ y(t) &= C_m x(t),\end{aligned} \tag{3.4}$$

where $x(t) = [\theta(t), q(t), x_{I1}(t), x_{I2}(t)]^\top$ is the vector of the system states, $r(t) = \theta_c(t)$ is the reference attitude command, $f_1(t,x) : \mathbb{R} \times \mathbb{R}^4 \to \mathbb{R}$ is a nonlinear function containing information on the residual of the feedforward torque compensation for the disturbance torque from the manipulator and the matched uncertainty, $f_2(t,x) : \mathbb{R} \times \mathbb{R}^4 \to \mathbb{R}^3$ is a nonlinear function representing additional modeling uncertainty, $A_m \in \mathbb{R}^{4\times4}$ is a known Hurwitz matrix defining the desired system dynamics, $B_r \in \mathbb{R}^{4\times1}$ is the known command matrix, $B_m \in \mathbb{R}^{4\times1}$ is the known control matrix, $C_m \in \mathbb{R}^{1\times4}$ is a known full-rank constant matrix, and $B_{um} \in \mathbb{R}^{4\times3}$ is a matrix such that $B_m^\top B_{um} = 0$ and $[B_m\ B_{um}]$ has full rank. The product $B_{um} f_2(t,x)$ represents the unmatched uncertainty. The matrices A_m, B_r, and B_m can be written as

$$A_m = \begin{bmatrix} 0 & 1 & 0 & 0 \\ -\frac{k_{P1}k_{P2}}{J_0} & \frac{k_{P1}k_D}{J_0} & \frac{k_{I1}}{J_0} & \frac{k_{P1}k_{I2}}{J_0} \\ -k_{P2} & k_D - 1 & 0 & k_{I2} \\ -1 & 0 & 0 & 0 \end{bmatrix}, \quad B_r = \begin{bmatrix} 0 \\ \frac{k_{P1}k_{P2}}{J_0} \\ k_{P2} \\ 1 \end{bmatrix}, \quad B_m = \begin{bmatrix} 0 \\ \frac{1}{J_0} \\ 0 \\ 0 \end{bmatrix}.$$

For the system given in 3.4, the following $\mathcal{L}_1$ adaptive controller is proposed.

3.4.1 State Predictor

Taking the same structure as the system in 3.4, the state predictor is given by

$$\dot{\hat{x}}(t) = A_m \hat{x}(t) + B_r r(t) + B_m \left(u_a(t) + \hat{\sigma}_1(t)\right) + B_{um} \hat{\sigma}_2(t), \quad \hat{x}(0) = x_0, \tag{3.5}$$

where $\hat{x}(t)$ is the predictor state, $\hat{\sigma}_1(t) \in \mathbb{R}$ and $\hat{\sigma}_2(t) \in \mathbb{R}^3$ are the estimates of the nonlinear functions $f_1(\cdot)$ and $f_2(\cdot)$ respectively.

3.4.2 Adaptation Law

Given an adaptation rate $T_s > 0$, the estimates $\hat{\sigma}_1(t)$ and $\hat{\sigma}_2(t)$ are updated according to the following piecewise constant adaptation law:

$$\begin{bmatrix} \hat{\sigma}_1(t) \\ \hat{\sigma}_2(t) \end{bmatrix} = \begin{bmatrix} \hat{\sigma}_1(iT_s) \\ \hat{\sigma}_2(iT_s) \end{bmatrix}, \quad t \in [iT_s, (i+1)T_s)$$
$$\begin{bmatrix} \hat{\sigma}_1(iT_s) \\ \hat{\sigma}_2(iT_s) \end{bmatrix} = -\begin{bmatrix} 1 & 0 \\ 0 & \mathbb{I}_3 \end{bmatrix} [B_m \; B_{um}]^{-1} \Phi^{-1}(T_s) e^{A_m T_s} \tilde{x}(iT_s), \quad i = 0, 1, 2, 3, ..., \tag{3.6}$$

where

$$\Phi^{-1}(T_s) = A_m^{-1} \left(e^{A_m T_s} - \mathbb{I}_4 \right)$$

and $\tilde{x}(t) = \hat{x}(t) - x(t)$ is the state prediction error.

3.4.3 Control Law

The control law is generated as the output of the following system:

$$u_a(s) = -k_a D(s) \hat{\eta}(s), \tag{3.7}$$

where $\hat{\eta}(s)$ is the Laplace transform of the signal

$$\hat{\eta}(t) \triangleq u_a(t) + \hat{\eta}_1(t) + \hat{\eta}_2(t)$$

with $\hat{\eta}_1(t) = \hat{\sigma}_1(t)$ and $\hat{\eta}_2(s) = H_1^{-1}(s) H_2(s) \hat{\sigma}_2(s)$ and

$$H_1(s) = C_m(s\mathbb{I} - A_m)^{-1} B_m,$$
$$H_2(s) = C_m(s\mathbb{I} - A_m)^{-1} B_{um}.$$

Here k_a is a feedback gain and $D(s)$ is a strictly proper transfer function, which lead to a strictly proper stable

$$C(s) \triangleq \frac{k_a D(s)}{1 + k_a D(s)}$$

with DC gain $C(0) = 1$.

3.5 State Estimation

This combination of feedforward and feedback control, especially the feedforward component, relies strongly on a good estimate of system states. It is often desirable to start with these lower fidelity models in order to facilitate the control design and testing.

The quadrotor system used in this work contains a 6-DOF Inertial Measurement Unit (IMU), a magnitometer, and a barometer onboard the vehicle. In addition to the onboard sensors, an external motion capture system is used for position feedback.

3.5.1 Complementary Angular Acceleration Estimation

While some states like position, acceleration, and angular velocity can be measured directly, other states such as translational velocity, orientation, and angular acceleration can be much harder to find. For the purpose of finding manipulator torques, we must have an accurate estimate of the angular acceleration of the vehicle about its pitch axis. To achieve this, we design a complementary filter, based on [18], using gyroscope measurements and knowledge of the dynamics of the system. First, the model predictive portion of the estimator must be constructed.

From knowledge of the vehicle's inertial properties and gyroscope measurement, we have

$$\hat{\dot{q}} = \frac{(I_{zz} - I_{xx})\, pr + I_{xz}\,(r^2 - p^2)}{I_{yy}} + \frac{\hat{M}_q}{I_{yy}},$$

where $I_{xx}, I_{yy}, I_{zz}, I_{xz}$ are elements of the vehicle inertia matrix, p, r are roll rate and yaw rate respectively, and $\hat{M}_q$ is the total estimated pitch moment on the airframe. Then, the complementary filter can be written as

$$\hat{\dot{\omega}}(s) = \frac{1}{1 + G(s)H(s)}\dot{\omega}_1(s) + \frac{G(s)H(s)}{1 + G(s)H(s)}\dot{\omega}_2(s),$$

and since $G(s)\dot{\omega}_2(s)$ is the gyroscope measurement, we have

$$\hat{\dot{\omega}}(s) = \frac{1}{1 + G(s)H(s)}\dot{\omega}_1(s) + \frac{H(s)}{1 + G(s)H(s)}\dot{\omega}_2(s).$$

Taking $G(s)$ to be an integrator and $H(s)$ to be a PI controller, we have

$$\hat{\dot{\omega}}(s) = \frac{s^2}{s^2 + K_P s + K_I}\dot{\omega}_1(s) + \frac{K_P s + K_I}{s^2 + K_p s + K_I}\left(s\omega_2(s)\right),$$

where K_P, K_I are proportional and integral gains for $H(s)$ respectively, and $\dot{\omega}_1$ is the estimated value from the model predictive estimator. Figures (3.3) and (3.4) illustrate the efficacy of this method as compared with purely using a backward difference estimator with a gyroscope measurement.

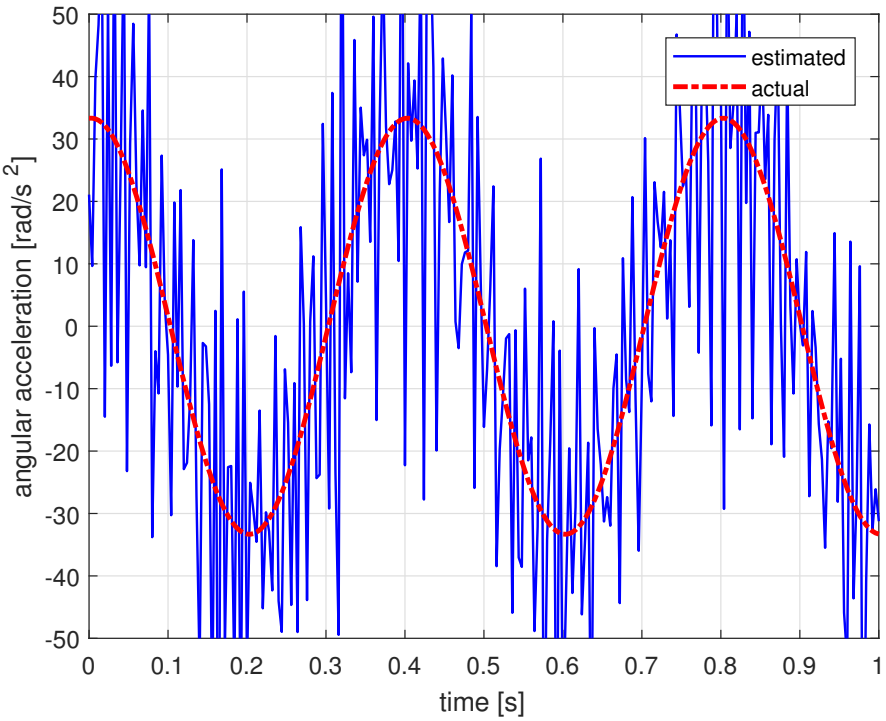

Figure 3.3: Angular acceleration - backward difference estimation

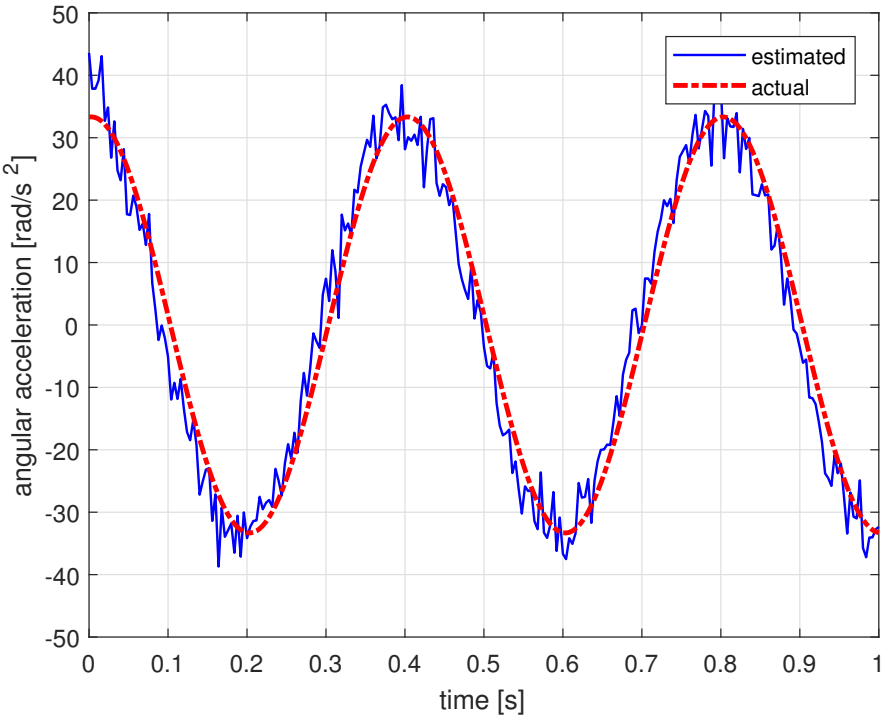

Figure 3.4: Angular acceleration - Complementary filter estimation

CHAPTER 4

VEHICLE DESIGN

4.1 Quadrotor Design

The design of a UAV that is both compact and powerful is essential for indoor manipulation and the interaction with humans. Therefore, for this application a useful metric by which to measure the effectiveness of a UAV is thrust-to-weight ratio. The main design goal for this UAV was to achieve the highest possible thrust-to-weight ratio while also satisfying constraints such as size, flight time, payload, etc. The resulting UAV achieves a maximum total thrust exceeding 1.6 kg yielding an expected thrust-to-weight ratio greater than 7 before the addition of a manipulator.

4.1.1 Frame

In order to achieve this desired thrust to weight ratio, a single layer of 2 mm carbon fiber sheet was used in the construction of the entire frame. Cross braces between arms act to both strengthen the frame as well as protect the propellers from ground strike. The modular design of the frame enables easy addition of accessories such as propeller guards, cameras, sensors, etc. A mounting plate on the underbelly of the frame is supported with four fixtures and is the connecting point for the manipulator. In the event of a crash involving the manipulator, the fixtures break away under high load to prevent damage to the quadrotor or manipulator.

4.1.2 Motors

The motors used in this quadotor were the Tiger Motor MT-1306 brushless motors with a KV value of 3100 and an operating voltage of 3S. The factory

recommendation for these motors is to use either 1S or 2S, however, a 3S battery can be used if the time at which the throttle is above $\frac{2}{3}$ is reserved for short bursts.

4.1.3 Propellers

Due to the fact that this vehicle is designed to be flown in indoor environments, sound was considered when choosing propellers. A 2-blade and 3-blade version of both a polymer and carbon fiber 5x3 propeller were tested at various throttle levels and the carbon fiber 3-blade made significantly less acoustic noise than the 2-blade version of both materials as well as the polymer 3-blade version. Thrust profiles of each propeller were also taken and since the variants performed almost identically, the carbon fiber 3-blade configuration was chosen.

4.1.4 Battery

An 800 mAh, 3S (11.1 V) lithium-polymer battery provides a flight time of approximately 10 minutes at a steady hover. In order to supply the necessary current to the motors, a battery with a 40C discharge rate was chosen.

Figure 4.1: Small quadrotor used in aerial manipulator

4.1.5 Flight Control Board

The flight controller for this quadrotor is from the CrazyFlie 2.0 nano quadcopter, adapted to command brushless motor ESCs through the use of a Bitcraze Bigquad Deck. This hardware was chosen for its open-source firmware, exceptional sensor quality, onboard state estimation, and small size. The structure of the stabilizing flight controller is a cascaded PID scheme taking inputs of desired attitude and giving outputs of desired body torque, ultimately corresponding to propeller motor velocities. Although the original configuration of the flight controller tuned for the CrazyFlie 2.0 did stabilize the larger vehicle, re-tuning was done to achieve more responsive and robust tracking performance.

4.2 Manipulator Design

The manipulator links were designed with an open truss structure in order to decrease weight while maintaining structural rigidity. Utilizing rapid

prototyping methods, the sections of the manipulator can be designed and manufactured to the exact specifications desired, without the geometric limitations of using carbon fiber. The two motors for the manipulator arm are fixed in the same reference frame and mounted to the quadrotor itself at the first joint. This configuration counterbalances the arm to ensure that the center of mass will remain close to the geometric center of the system, even with payload far from the center. One of these two motors is used to actuate the second joint, where the second link is attached. A cable system is run from the second servo motor through the inside of the first link to the second joint. At the end of the second link, the end effector is mounted.

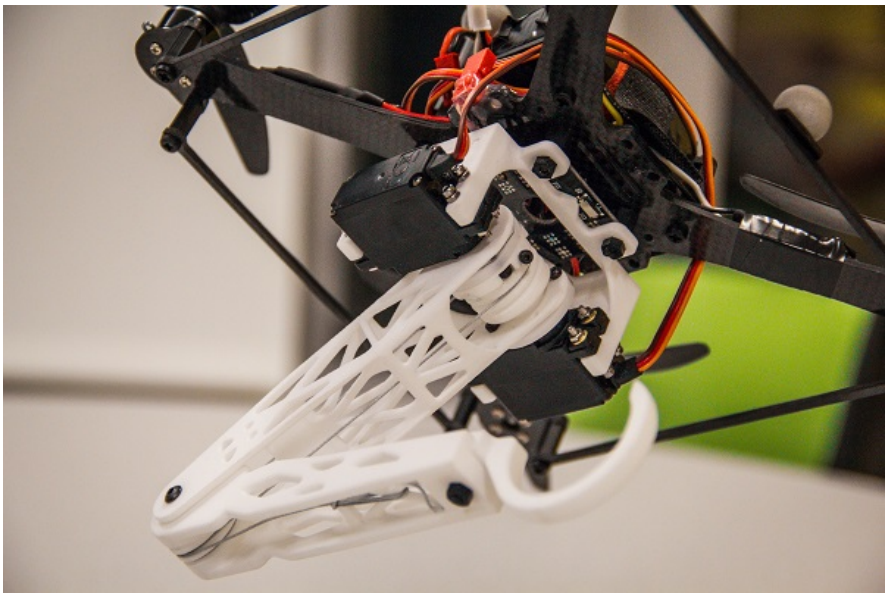

Figure 4.2: Manipulator link design and cable actuation system

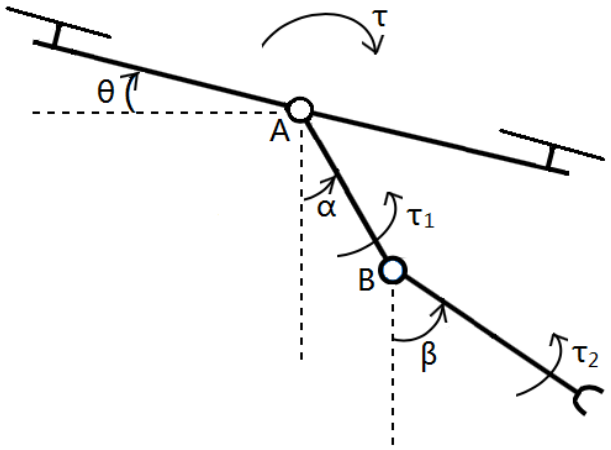

Figure 4.3: Diagram of the UAS in the symmetric plane

The manipulator was designed using globally defined joint angles, as seen in Figure 4.3, which translate to independent orientations between both links. This topology is useful for maintaining the manipulator center of mass closer to its base, however, it also introduces an undesirable behavior where the workspace is reduced and is defined by geometric relationships of added complexity. One method of calculating the workspace, in this case, is to define the region using sweeps of limit configurations for each joint. For this design, the calculated workspace is shown in Figure 4.4. This unusual shape is due to physical limitations of each link and actuators in conjunction with the globally defined angles.

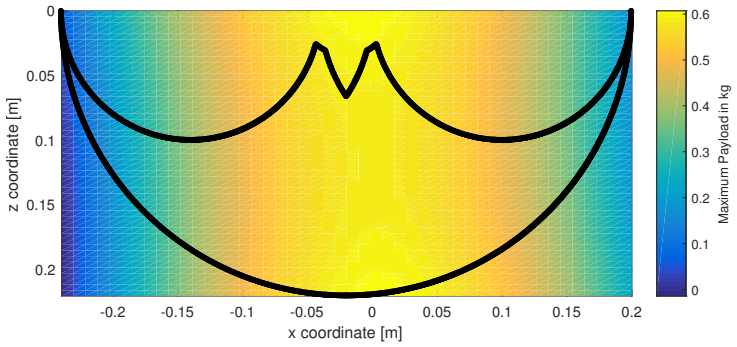

Figure 4.4: UAS payload plot (heatmap) overlaid by manipulator workspace (line)

CHAPTER 5

EXPERIMENTATION

Two methods of experimentation were carried out to validate the efficacy of this control augmentation scheme. The first was a high-fidelity simulation of the quadrotor and manipulator dynamics using MATLAB Simulink. The second was the implementation of the control scheme on a real quadcopter with a 2-link manipulator.

5.1 Simulation Results

Simulations were carried out in the MATLAB Simulink environment using a desktop workstation running MATLAB version 8.5-9.2 in Windows 7 with an Intel Core i7-4790 CPU and 16 GB RAM. Quadrotor dynamics were simulated using the included Custom Variable Mass 6DOF (Quaternion) block. Simulations were run with a variable time step solver.

5.1.1 Baseline Controller

The first set of results illustrates the step response of the rate and attitude CAS's for the PI baseline controller described in Chapter 3.

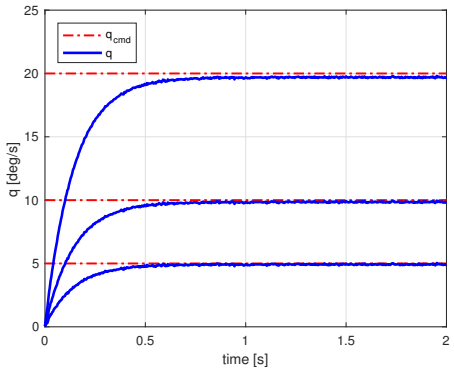

(a) Step response of rate CAS

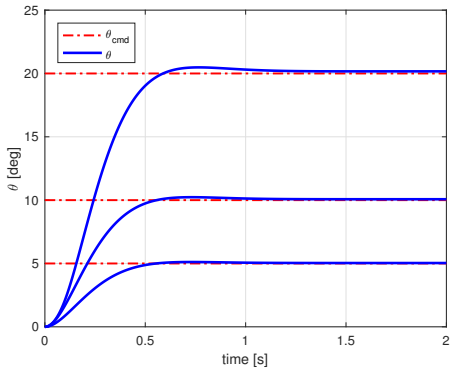

(b) Step response of attitude CAS

Figure 5.1: Step response of baseline controller

5.1.2 Feedforward Torque Compensation

This section uses the simulation of the baseline PI controller augmented with the feedforward torque compensator to track a zero pitch reference while the manipulator transitions from a fully forward reaching configuration to a fully backward reaching configuration in 1 second with no payload.

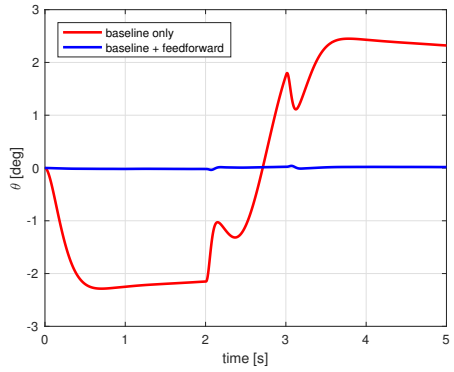

(a) Attitude angle during manipulator motion

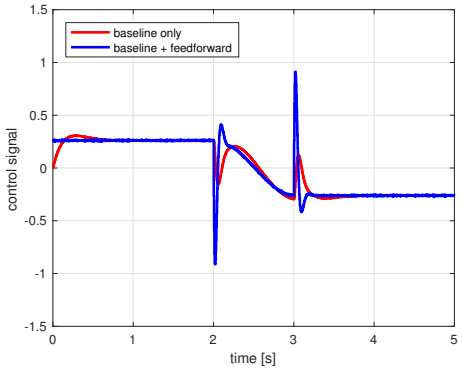

(b) Control signal during manipulator motion

Figure 5.2: Performance of the feedforward compensation

One might expect to see attitude tracking performance on this order of magnitude since we are compensating for a very well known system.

5.1.3 $\mathcal{L}_1$ Adaptive Augmentation

Now, an unmodelled payload of 25 grams is added to the end effector and two different scenarios are executed, shown in 5.3. The three output plots represent the performance of the uncompensated baseline controller, the feed-forward augmented baseline controller, and the $\mathcal{L}_1$-augmentation of the baseline.

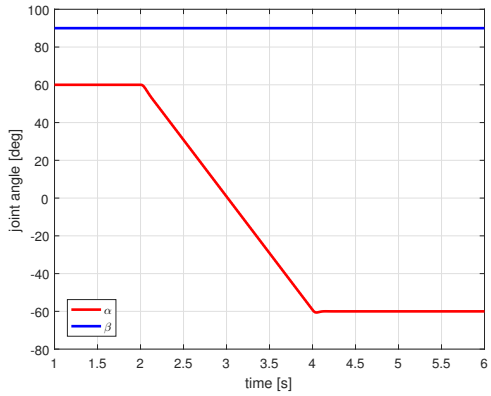

(a) Manipulator angles, scenario 1

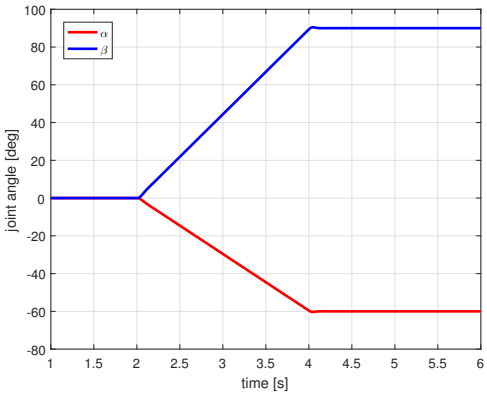

(d) Manipulator angles, scenario 2

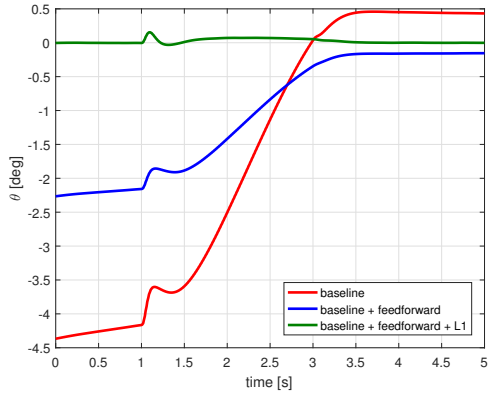

(b) Pitch angle, scenario 1

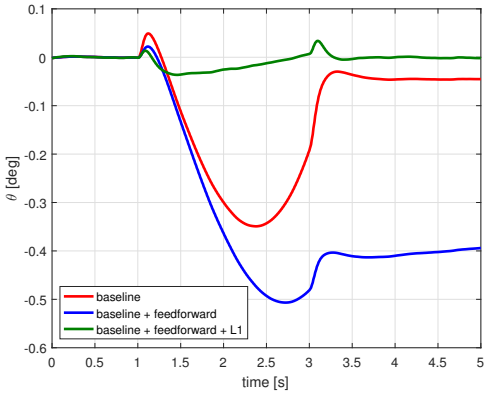

(e) Pitch angle, scenario 2

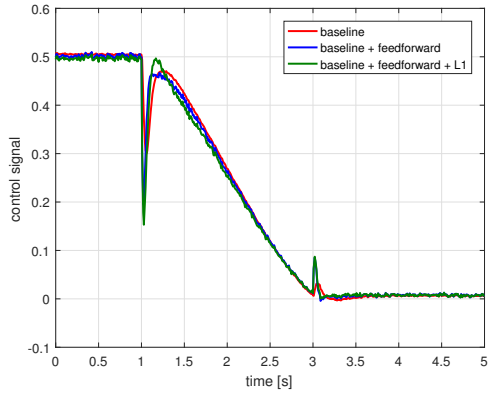

(c) Control signal, scenario 1

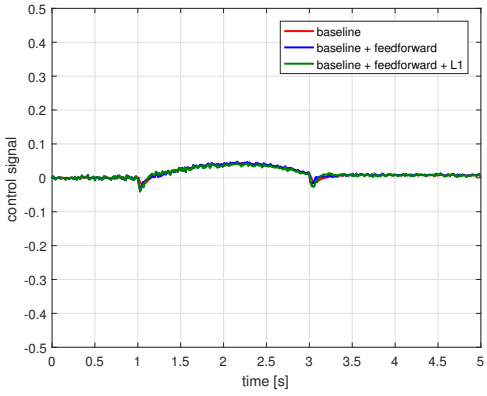

(f) Control signal, scenario 2

Figure 5.3: Performance of the $\mathcal{L}_1$ adaptive augmentation

One can see that even in the presence of manipulator torque and unknown payloads, the baseline controller with feedforward and $\mathcal{L}_1$ performs extremely well.

5.2 Flight Testing

5.2.1 Flight Arena

All flight tests were conducted in an 8 x 8 x 4 m fully netted flight arena. Eight Vicon T40 motion capture cameras were used to capture the position of the vehicle at 240 Hz. While the motion capture camera system can return orientation of objects in the arena, these measurements were not used.

The following plots are broken down into groups of three scenarios, testing the effectiveness of the feedforward torque compensation part of the augmenting controller. The following test results were carried out with both links of the manipulator tracking the same angle command. The geometric baseline controller was chosen and was designed to track a position 1 meter above the origin. The first half of the trials are with no payload and the second half use a modeled payload of 25 grams.

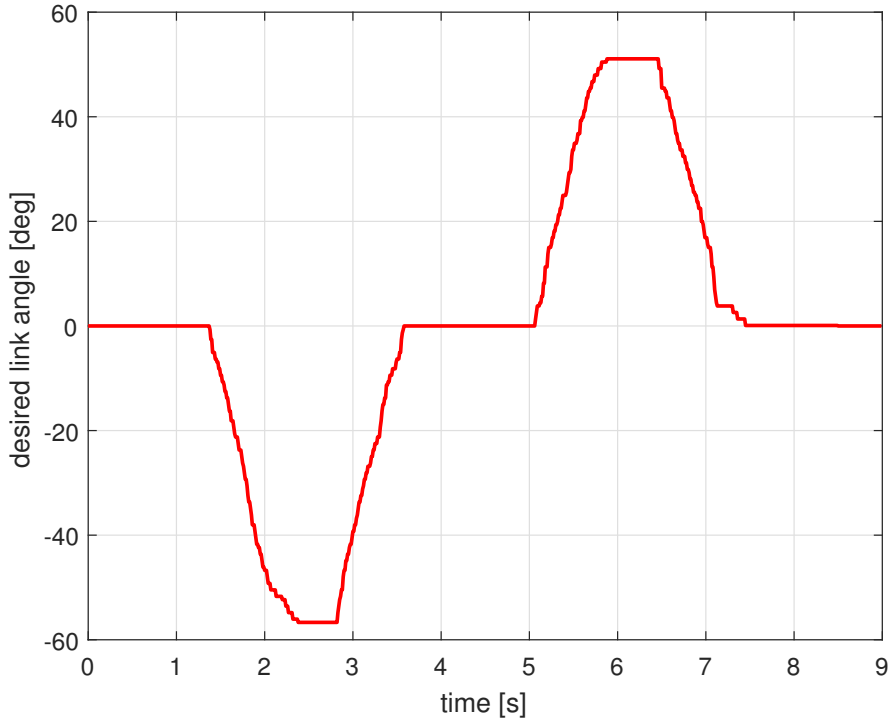

Figure 5.4: Manipulator command - baseline controller with no payload

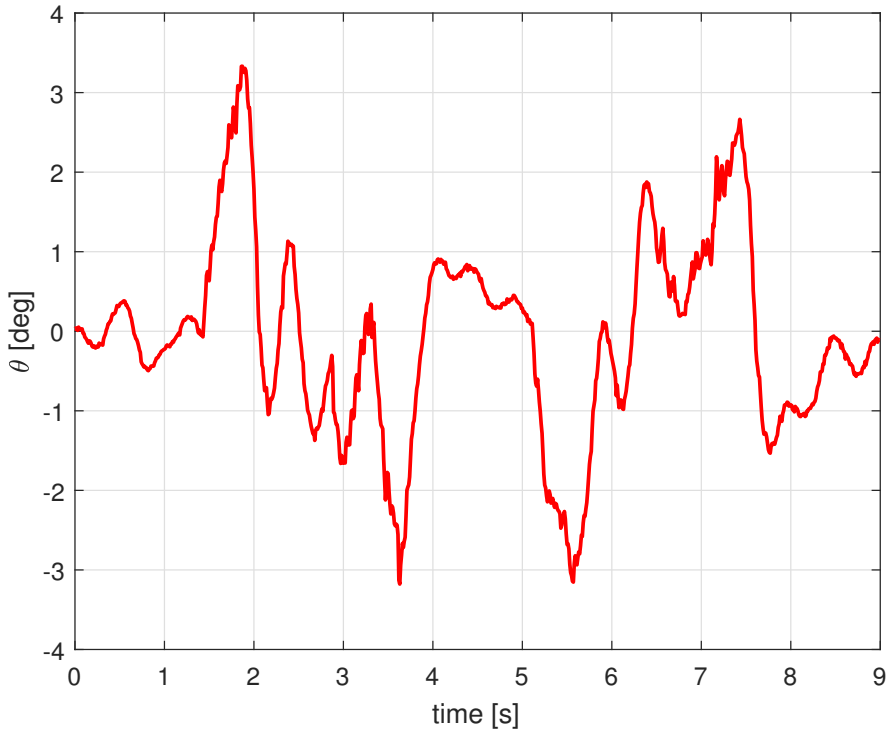

Figure 5.5: Pitch response - baseline controller with no payload

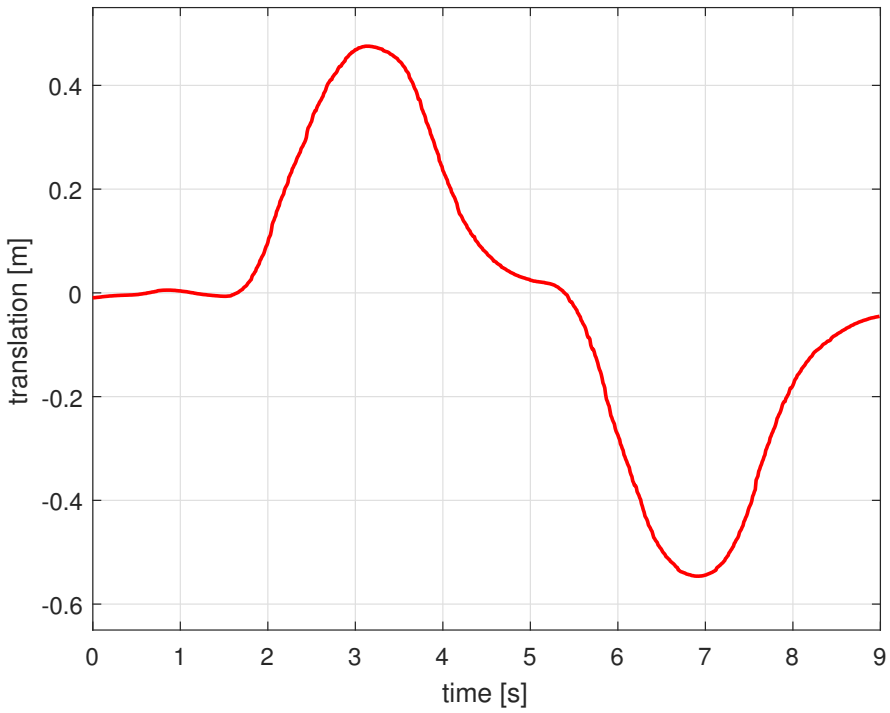

Figure 5.6: Translation response - baseline controller with no payload

We can see that with no compensation of the baseline controller the desired attitude and position are tracked very poorly. With the manipulator fully extended, the baseline controller cannot overcome the steady state error, and the translation exceeds 0.5 m.

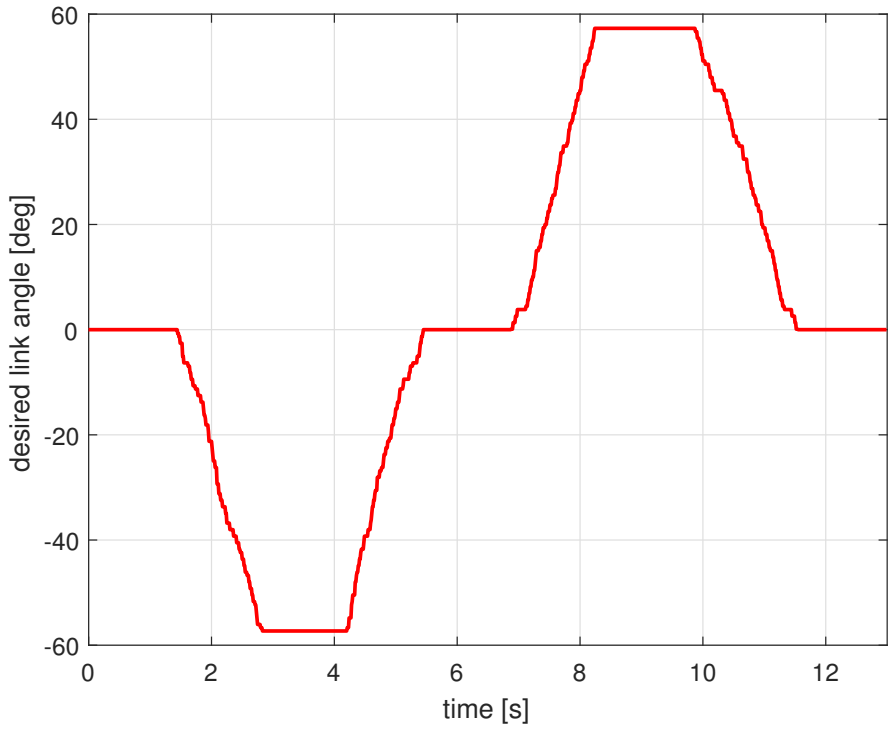

Figure 5.7: Manipulator command - static compensation with no payload

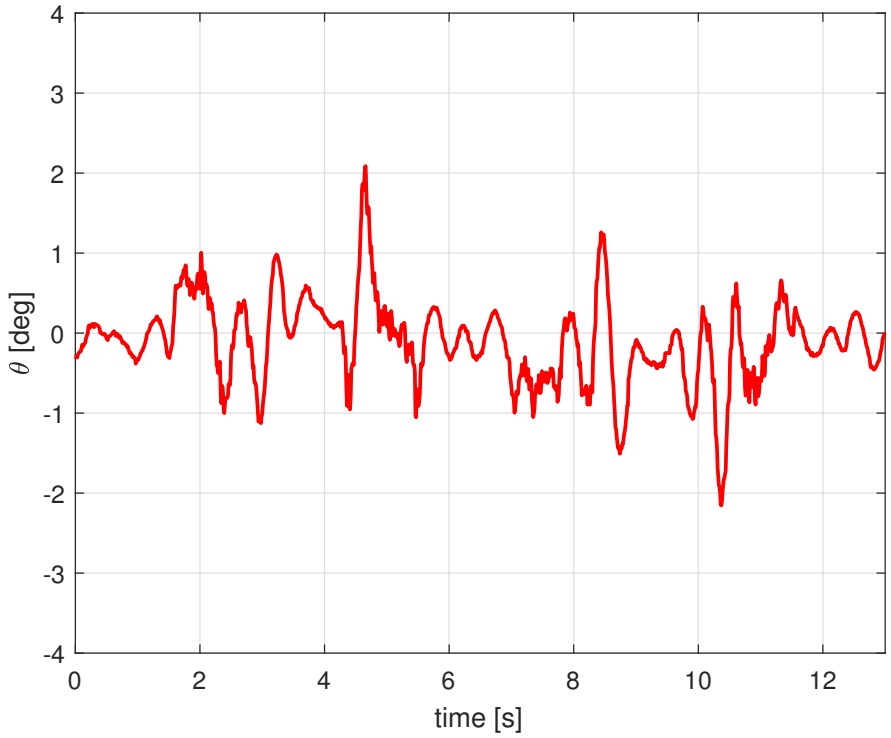

Figure 5.8: Pitch response - static compensation with no payload

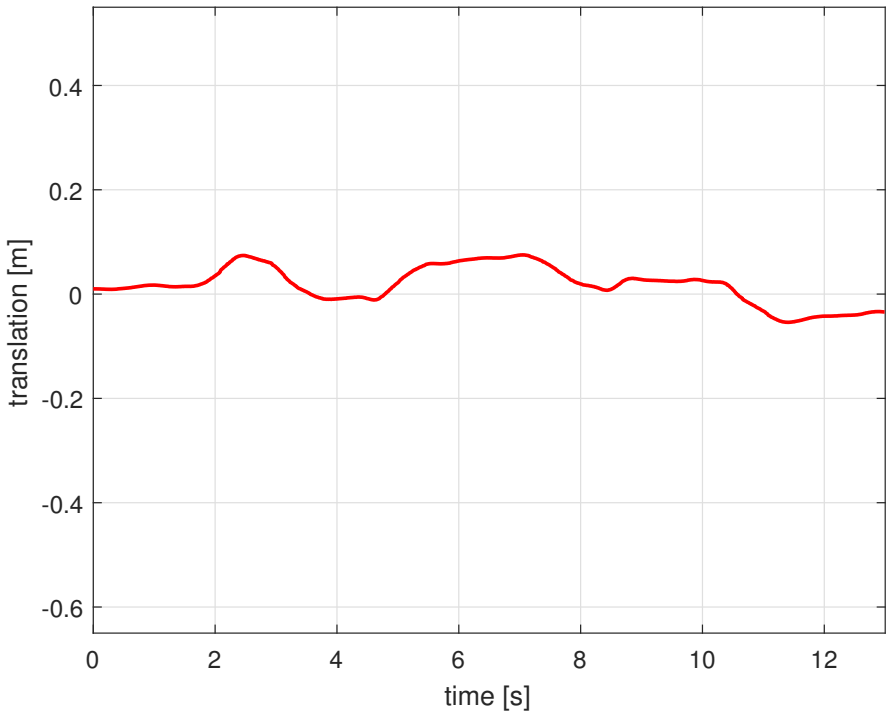

Figure 5.9: Translation response - static compensation with no payload

In this trial, only the static component of the feedforward signal is used, and we can see immediately the significant improvement in baseline tracking.

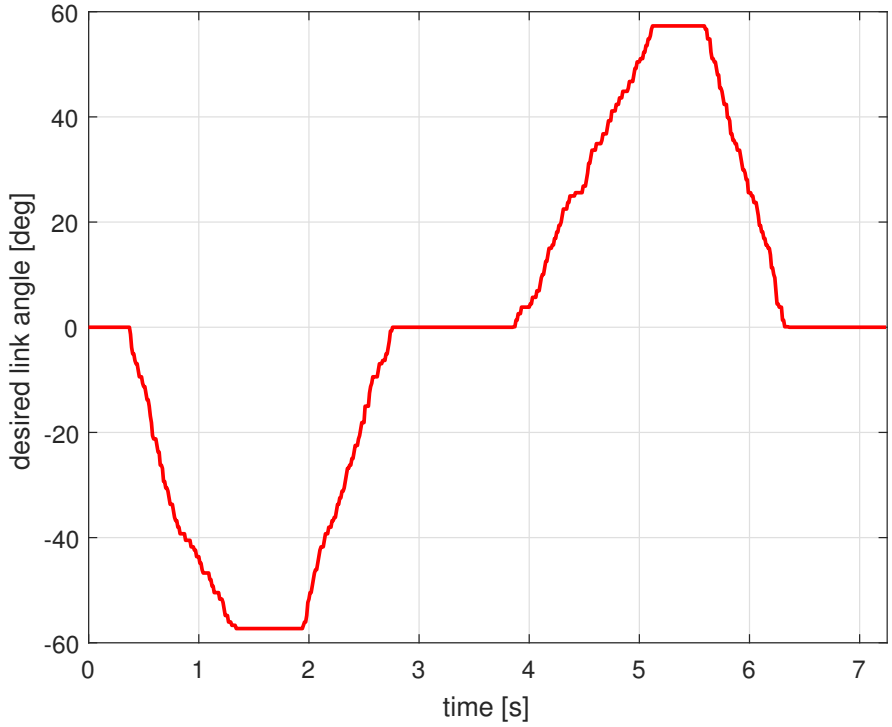

Figure 5.10: Manipulator command - full compensation with no payload

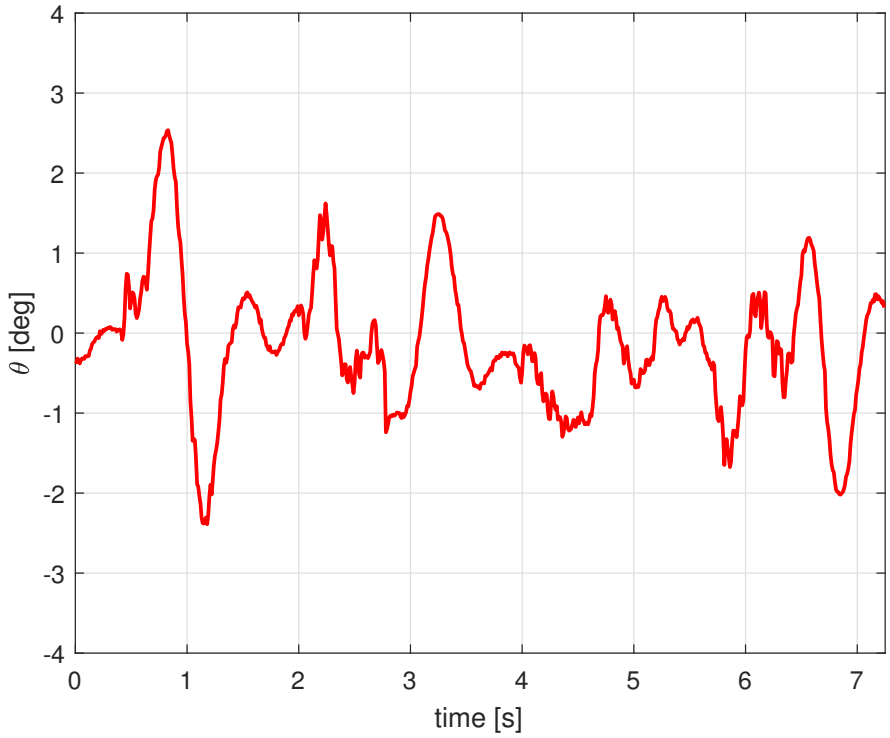

Figure 5.11: Pitch response - full compensation with no payload

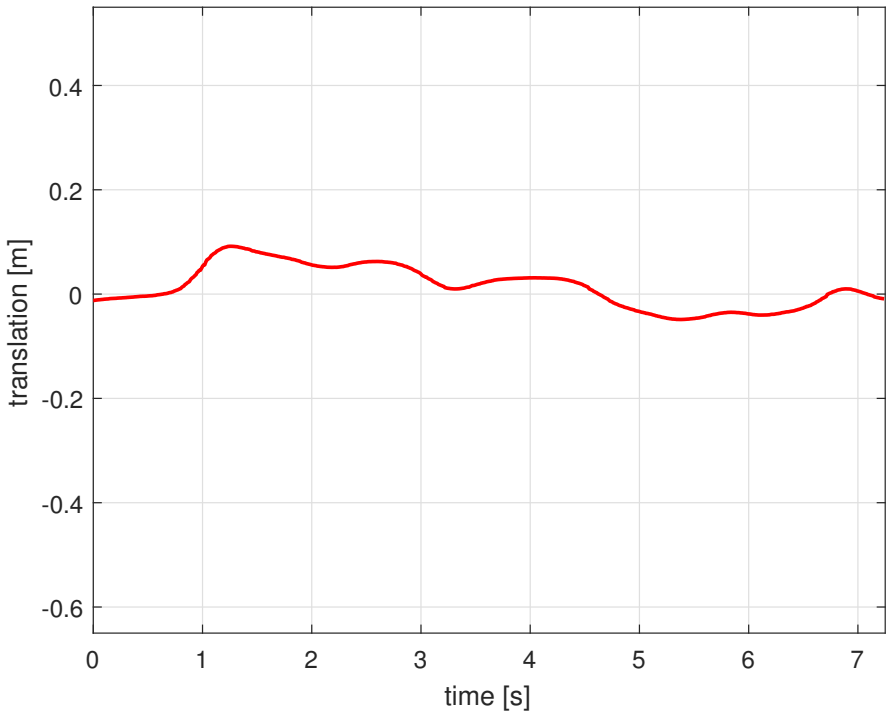

Figure 5.12: Translation response - full compensation with no payload

With the use of the entire feedforward signal attitude errors are slightly increased, however, position tracking performance remains much better than the baseline-only scenario.

The following plots show the flight performance when a 25 gram payload is added to the end effector.

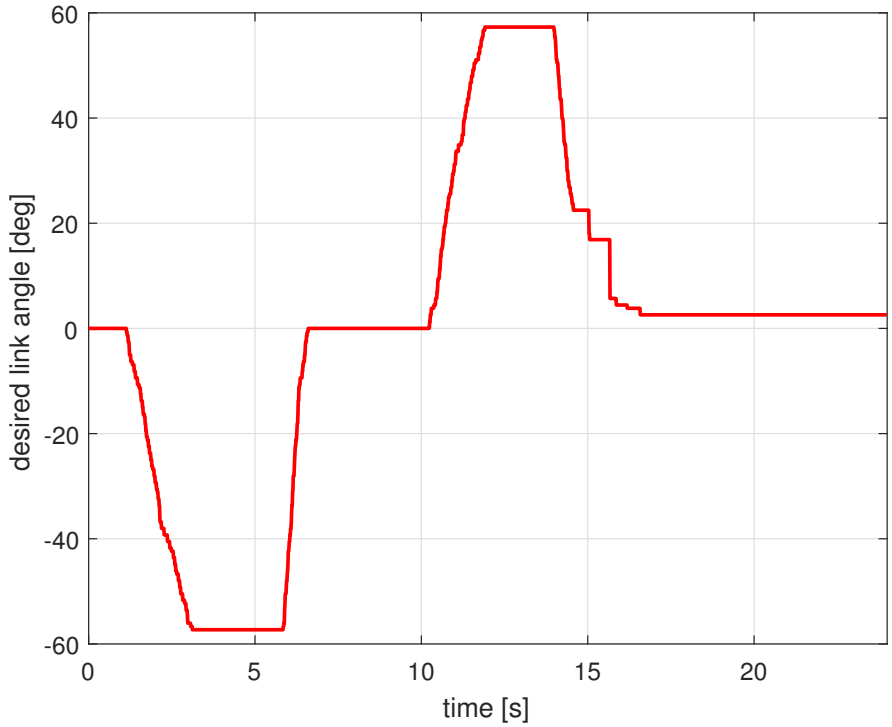

Figure 5.13: Manipulator command - baseline controller with payload

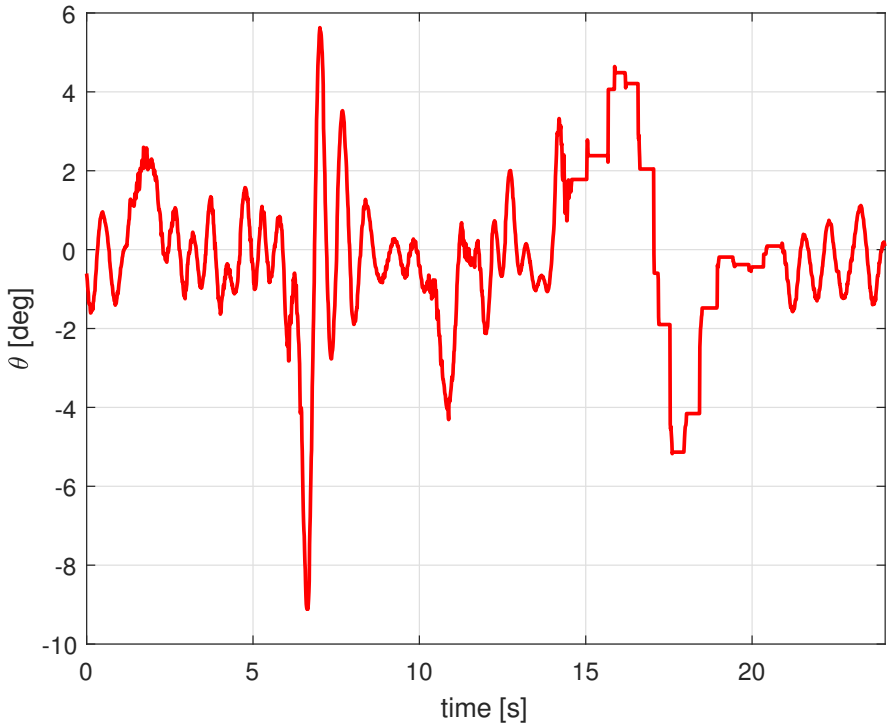

Figure 5.14: Pitch response - baseline controller with payload

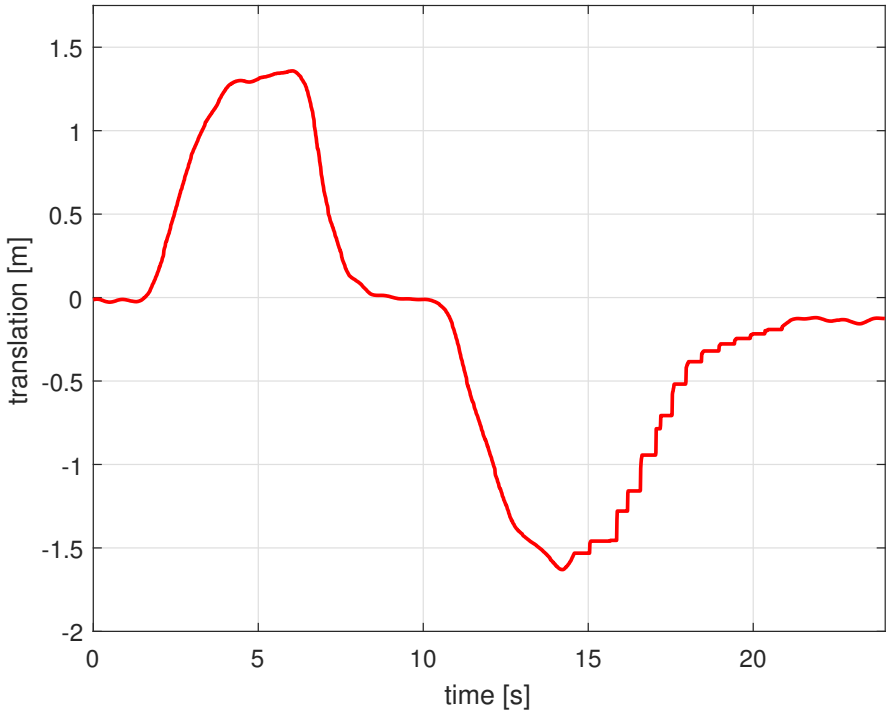

Figure 5.15: Translation response - baseline controller with payload

It is obvious that the addition of a payload would increase the moments induced on the quadrotor and therefore, we would expect to see tracking errors to increase as well. This is, in fact, the case seen above.

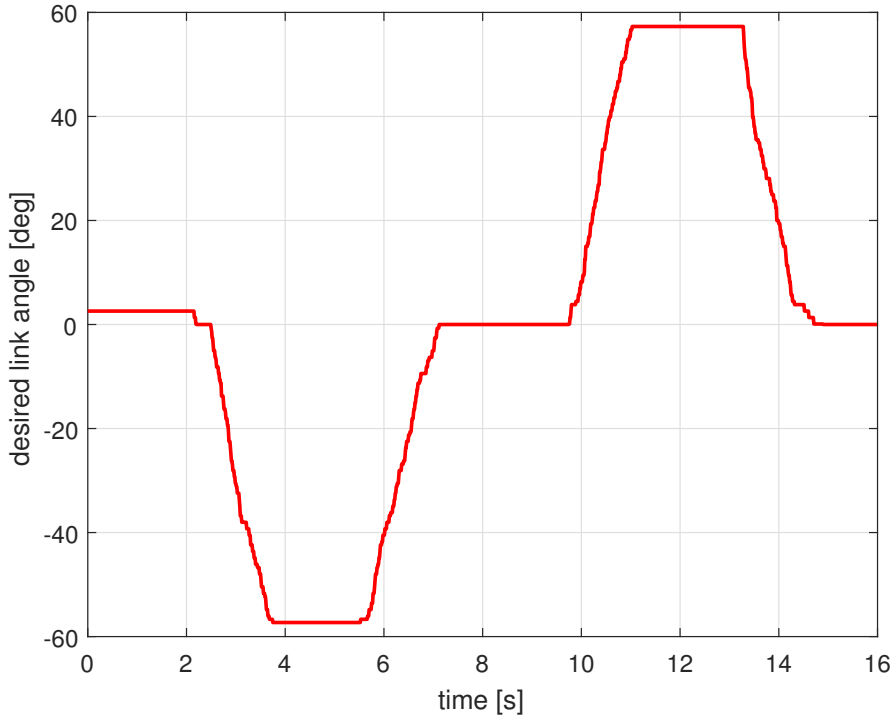

Figure 5.16: Manipulator command - static compensation with payload

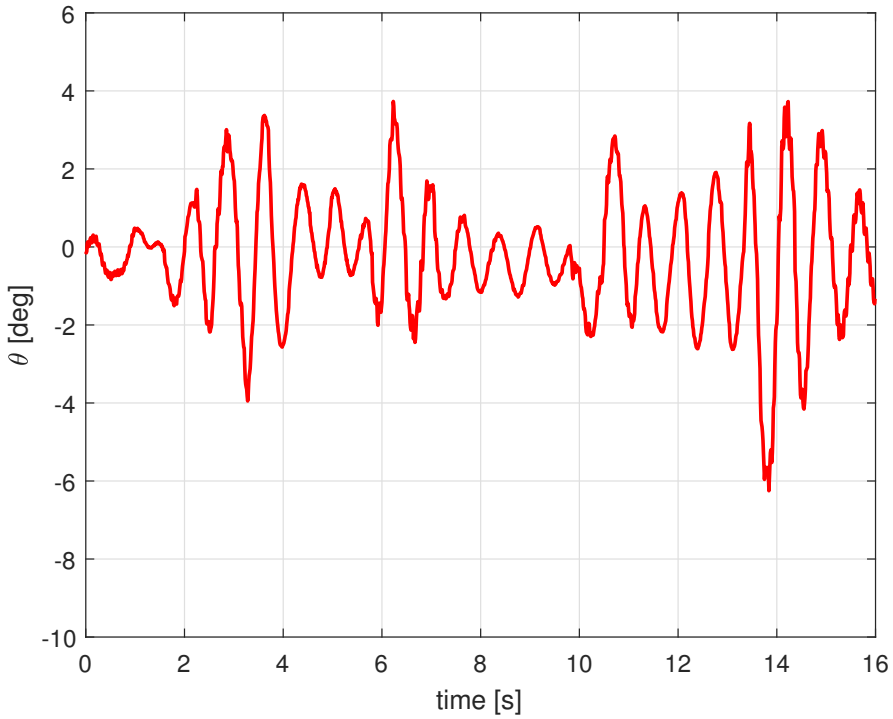

Figure 5.17: Pitch response - static compensation with payload

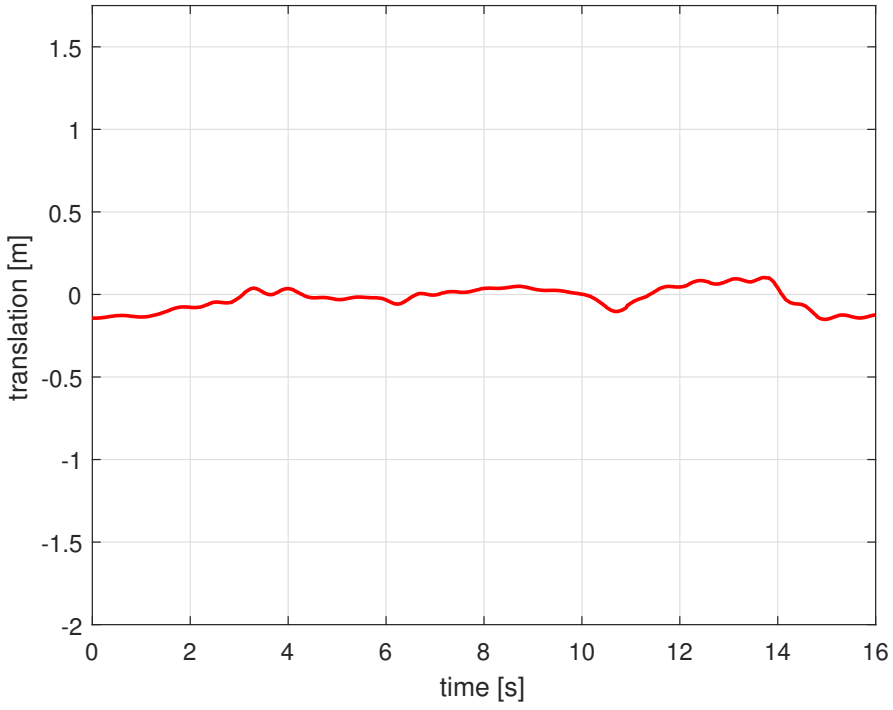

Figure 5.18: Translation response - static compensation with payload

In the static only case, we can notice data loss during flight logging between 14 and 21 seconds, however, the overall trend is still visible.

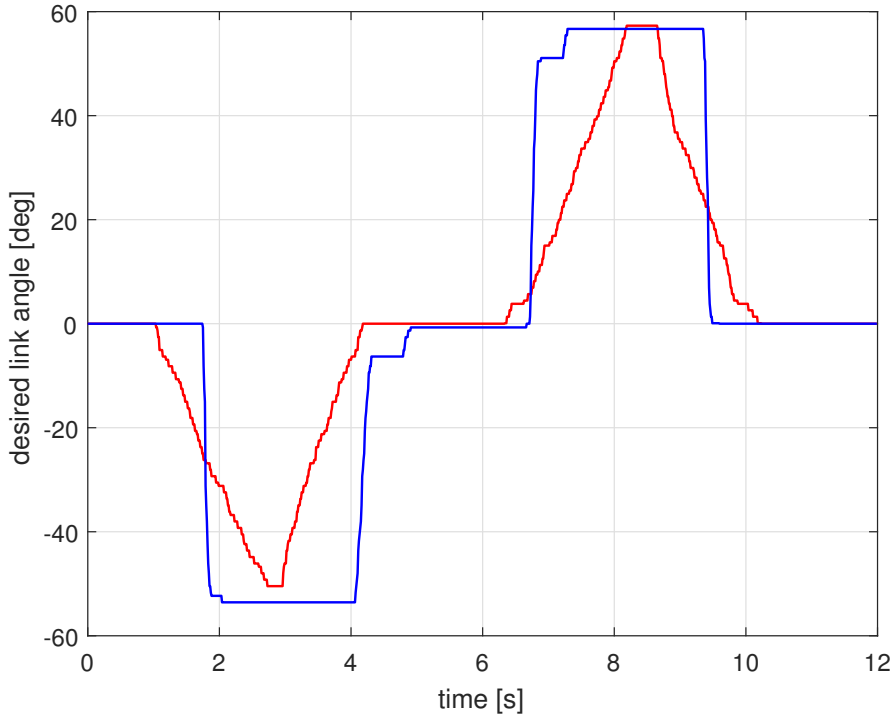

Figure 5.19: Manipulator command - full compensation with payload

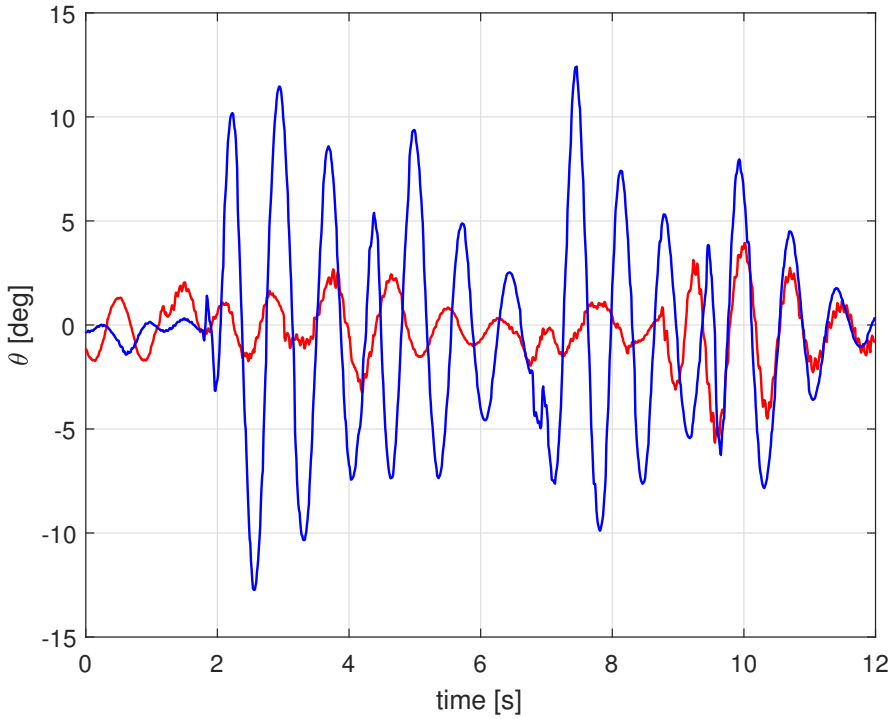

Figure 5.20: Pitch response - full compensation with payload

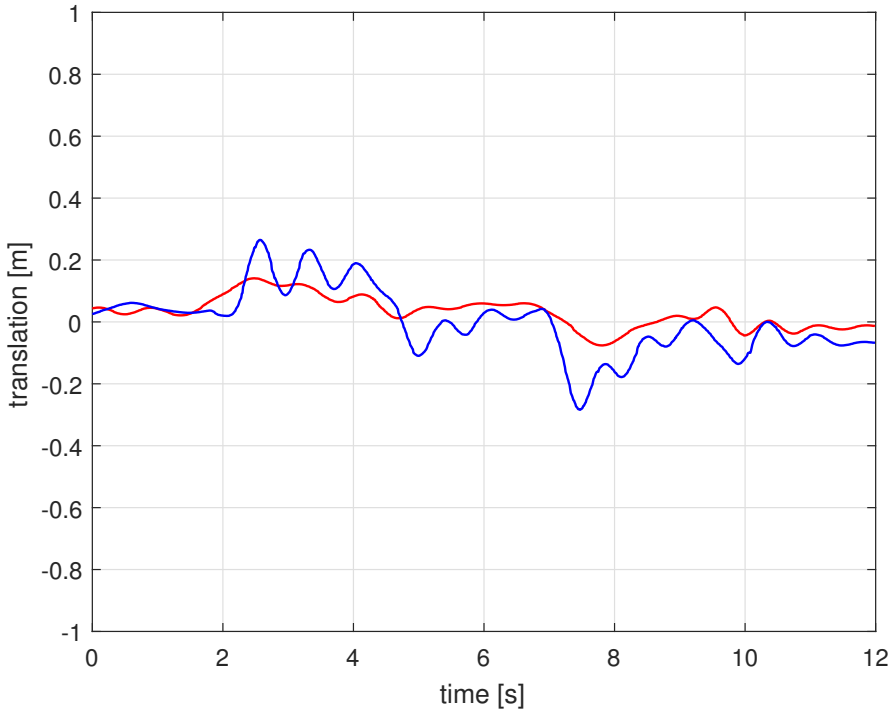

Figure 5.21: Translation response - full compensation with payload

The last scenario demonstrates the true effectiveness of the feedforward torque compensation scheme. Shown in blue, a desired maneuver with high angular velocity and acceleration is executed. Due to unmodeled forces acting on the translational dynamics of the vehicle, the geometric position tracking controller needed to relinquish orientation tracking to achieve a desired position. Nonetheless, the position tracking error is kept much smaller than that of the baseline controller only.

CHAPTER 6

CONCLUSION

6.1 Summary

This thesis aimed to improve the state-of-the-art in mobile manipulators through the use of smart hardware design and advanced control methods. It presented a mathematical framework in which vehicle performance was studied. It proposed an augmenting control structure accounting for a known manipulator and unknown payloads. It discussed the design methodology for an actual aerial manipulator which was built and flown. Lastly, it presented results from simulation and flight tests verifying the efficacy of the proposed vehicle design and control scheme.

6.2 Future Work

While this thesis showed positive results for both the aerial manipulator design and augmenting control scheme, aspects of both would need further investigation if this proposed system were to be adopted by a larger community.

A more complete dynamic model would serve to capture currently unmodeled dynamic phenomena, such as centripetal forces induced onto the airframe by the manipulator during high angular velocity maneuvers. The augmentation of a baseline controller proposed in this work also does not consider the effects generated by the manipulator in the roll or yaw direction. A complete representation of the aerial manipulator as a single system, rather than two dynamically coupled subsystems, would allow for better utilization of actuator capabilities and less conservative controllers.

Manipulator actuators with position feedback and a greater range of motion

would allow for more accurate system knowledge and control, and provide a larger workspace for manipulation tasks.

REFERENCES

[1] "NRI: Collaborative research: ASPIRE: Automation supporting prolonged independent residence for the elderly," National Science Foundation, August 2015, http://www.nsf.gov/awardsearch/showAward?AWD_ID=1528036&HistoricalAwards=false [cited June 2016].

[2] T. L. Mitzner, C.-A. Smarr, J. M. Beer, T. L. Chen, J. M. Springman, A. Prakash, C. C. Kemp, and W. A. Rogers, "Older adults' acceptance of assistive robots for the home," Human Factors and Aging Laboratory, Georgia Institute of Technology, Technical Report HFA-TR-1105, 2011.

[3] D. Mellinger, Q. Lindsey, M. Shomin, and V. Kumar, "Design, modeling, estimation and control for aerial grasping and manipulation," in *2011 IEEE/RSJ International Conference on Intelligent Robots and Systems*. San Francisco, CA: Institute of Electrical & Electronics Engineers (IEEE), Sept 2011. [Online]. Available: http://dx.doi.org/10.1109/IROS.2011.6094871

[4] R. Spica, A. Franchi, G. Oriolo, H. H. Bulthoff, and P. R. Giordano, "Aerial grasping of a moving target with a quadrotor UAV," in *2012 IEEE/RSJ International Conference on Intelligent Robots and Systems*. Vilamoura, Algarve, Portugal: Institute of Electrical & Electronics Engineers (IEEE), Oct 2012. [Online]. Available: http://dx.doi.org/10.1109/IROS.2012.6385771

[5] A. Khalifa, M. Fanni, A. Ramadan, and A. Abo-Ismail, "Modeling and control of a new quadrotor manipulation system," in *2012 First International Conference on Innovative Engineering Systems*. Alexandria: Institute of Electrical & Electronics Engineers (IEEE), dec 2012. [Online]. Available: http://dx.doi.org/10.1109/ICIES.2012.6530854

[6] J. Thomas, J. Polin, K. Sreenath, and V. Kumar, "Avian-inspired grasping for quadrotor micro UAVs," in *Volume 6A: 37th Mechanisms and Robotics Conference*. Portland, Oregon: ASME International, Aug 2013. [Online]. Available: http://dx.doi.org/10.1115/DETC2013-13289

[7] J. Thomas, G. Loianno, J. Polin, K. Sreenath, and V. Kumar, "Toward autonomous avian-inspired grasping for micro aerial vehicles," *Bioinspir. Biomim.*, vol. 9, no. 2, p. 025010, May 2014. [Online]. Available: http://dx.doi.org/10.1088/1748-3182/9/2/025010

[8] M. Orsag, C. Korpela, S. Bogdan, and P. Oh, "Lyapunov based model reference adaptive control for aerial manipulation," in *2013 International Conference on Unmanned Aircraft Systems (ICUAS)*. Atlanta, GA: Institute of Electrical & Electronics Engineers (IEEE), may 2013. [Online]. Available: http://dx.doi.org/10.1109/ICUAS.2013.6564783

[9] D. Bazylev, A. Margun, K. Zimenko, and A. Kremlev, "UAV equipped with a robotic manipulator," in *22nd Mediterranean Conference on Control and Automation*. Palermo, Italy: Institute of Electrical & Electronics Engineers (IEEE), Jun 2014. [Online]. Available: http://dx.doi.org/10.1109/MED.2014.6961535

[10] T. W. Danko, K. P. Chaney, and P. Y. Oh, "A parallel manipulator for mobile manipulating UAVs," in *2015 IEEE International Conference on Technologies for Practical Robot Applications (TePRA)*. Woburn, MA: Institute of Electrical & Electronics Engineers (IEEE), May 2015. [Online]. Available: http://dx.doi.org/10.1109/TePRA.2015.7219682

[11] H. Lee, S. Kim, and H. J. Kim, "Control of an aerial manipulator using on-line parameter estimator for an unknown payload," in *2015 IEEE International Conference on Automation Science and Engineering (CASE)*. Gothenburg, Sweden: Institute of Electrical & Electronics Engineers (IEEE), aug 2015. [Online]. Available: http://dx.doi.org/10.1109/CoASE.2015.7294098

[12] G. Garimella and M. Kobilarov, "Towards model-predictive control for aerial pick-and-place," in *2015 IEEE International Conference on Robotics and Automation (ICRA)*. Seattle, WA: Institute of Electrical & Electronics Engineers (IEEE), May 2015. [Online]. Available: http://dx.doi.org/10.1109/ICRA.2015.7139850

[13] R. M. Jones, D. Sun, G. B. Haberfeld, A. Lakshmanan, T. Marinho, and N. Hovakimyan, "Design and control of a small aerial manipulator for indoor environments," in *AIAA Information Systems - AIAA Infotech @ Aerospace, AIAA SciTech Forum*. Grapevine, TX: American Institute of Aeronautics and Astronautics, January 2017.

[14] R. M. Murray, Z. Li, and S. S. Sastry, *A Mathematical Introduction to Robotic Manipulation*. Boca Raton, FL: CRC Press, 1994.

[15] T. Lee, M. Leoky, and N. H. McClamroch, "Geometric tracking control of a quadrotor uav on se(3)," in *49th IEEE Conference on Decision and Control (CDC)*, Dec 2010, pp. 5420–5425.

[16] A. Lakshmanan, "Piecewise Bézier Curve Trajectory Generation and Control for Quadrotors," M.S. thesis, University of Illinois at Urbana-Champaign, Dec. 2016.

[17] N. Hovakimyan and C. Cao, $\mathcal{L}_1$ *Adaptive Control Theory: Guaranteed Robustness with Fast Adaptation*. SIAM, 2010.

[18] Y. Jiali and Z. Jihong, "An angular acceleration estimation method based on the complementary filter theory," in *2016 IEEE International Instrumentation and Measurement Technology Conference Proceedings*, May 2016, pp. 1–6.